Pérez-Rodríguez *et al.*
Earth, Planets and Space (2019) 71:80
https://doi.org/10.1186/s40623-019-1059-x

Earth, Planets and Space

FULL PAPER Open Access

A comprehensive paleomagnetic study from the last Plinian eruptions of Popocatepetl volcano: absolute chronology of lavas and estimation of emplacement temperatures of PDCs

Nayeli Pérez-Rodríguez[1], Juan Morales[2*], Avto Goguitchaichvili[2] and Felipe García-Tenorio[3]

Abstract

Three lava flows (Buenavista, Xalitzintla and Nealtican) and pyroclastic density currents (Lorenzo and Pink Pumice) from two Popocatepetl Plinian eruptions were sampled for paleomagnetic dating. A detailed rock-magnetic characterization of the lavas, scoria clasts and pottery shards intercalated between the volcanic deposits was also carried out. Reliable results, both in direction and in intensity, were obtained for the Nealtican lava flow, which enabled its full-vector paleomagnetic dating using the archaeo_dating tool together with the global paleosecular variation model SHA.DIF.14 k, obtaining an age interval between 1040 AD and 1140 AD (95% probability confidence level), in good agreement with its associated ^{14}C age. The well-grouped paleomagnetic direction of the seven specimens from two different scoria clasts of the Lorenzo Pumice pyroclastic density current suggests that clasts were emplaced hot, at a temperature that seems to have almost completely erased the original remanent magnetization of the clasts. This fact is supported by the reheating of the underlying pottery shards, evidenced as a clear secondary low-temperature range (room temperature to 350 °C) component at the orthogonal vector plots. Similarly, the three mean clusters directions obtained for site PO-2 (Pink Pumice)—roughly concentrated around the present geomagnetic field—suggest also a high emplacement temperature. Also, the first archeointensity dating of a pottery shard within the pyroclastic density current is reported. Finally, results of the rock-magnetic and paleomagnetic dating of the last Plinian eruptions from the Popocatepetl volcano, applied to different volcanic materials (lava and pyroclastic density currents), show the usefulness of these nonconventional and alternative techniques in the study of the eruptive activity of volcanoes.

Keywords: Popocatepetl volcano, Plinian eruptions, Paleomagnetism, Paleointensity, Emplacement temperatures

*Correspondence: jmorales@geofisica.unam.mx
[2] Laboratorio Interinstitucional de Magnetismo Natural (LIMNA) y Servicio Arqueomagnético Nacional (SAN), Instituto de Geofísica, UNAM, Unidad Michoacán, Campus Morelia, Antigua Carretera a Pátzcuaro No. 8701 Col. Ex-Hacienda de San José de la Huerta, 58190 Morelia, Michoacán, Mexico
Full list of author information is available at the end of the article

Introduction

Popocatepetl is the riskiest volcano in Mexico, with nearly one million people living within a radius of 40 km (Macías 2005). It is located 65 km southeast from Mexico City—with almost 9 million inhabitants—and forms the southern end of the Sierra Nevada, consisting of Tlaloc, Telapón, Teyotl, Iztaccihuatl and Popocatepetl volcano. Popocatepetl means in Nahuatl "the smoking mountain"; this refers to the fact that, during the pre-Hispanic era, the Aztecs observed it in activity on several occasions.

Its eruptive history has been very explosive throughout the last 23 ka BP, recording at least five Plinian eruptions. In this period, the volcano experienced three destructive events; the last one occurred at 14 ka BP and gave rise to the construction of the present-day cone (Sosa-Ceballos et al. 2015). During the Holocene, the Popocatepetl had two eruptions that occurred during pre-Hispanic periods: Lorenzo Pumice (~2100 BP) and Pink Pumice (~1000 BP), which had implications on the human settlements in the basin of Puebla (Plunket and Uruñuela 1998). The eruptions were dated by the ^{14}C method in soils that inter-stratify with pyroclastic materials (Robin 1984; Siebe et al. 1996a; Plunket and Uruñuela 1998; Panfil et al. 1999; Siebe and Macías 2006; Arana-Salinas et al. 2010). However, several inconsistencies regarding the ^{14}C results and the lithological descriptions have not allowed to establish a definitive eruptive history (Siebe et al. 1995). In addition, it should be noted that the limited scope of lava flows (3 km from the top of the crater, on average) and the low impact they have on the evaluation of volcanic hazards has caused a low interest in their study, with little information generated on these.

Worth mentioning is that the radiocarbon method does not date the volcanic product directly, but the organic matter associated with an event of interest. On the contrary, the paleomagnetic method allows to obtain the absolute age of the lava flow's cooling moment based on the comparison of the geomagnetic field logged by the magnetic minerals within the volcanic rocks against a set of paleosecular variation (PSV) master curves established for the same geographical region, or by using geomagnetic field models calculated for the geographical region under study.

Nevertheless, few paleomagnetic studies have been devoted to the study of the Popocatepetl lava flows (e.g., Carrasco-Nuñez et al. 1986; Conte et al. 2004; Kosterov et al. 2009), while no paleodirection neither paleointensity studies have been reported on its pyroclastic deposits up to now, although successfully paleosecular variation studies have been reported on pyroclastic deposits from Mt. St. Helens, USA, Volcán Láscar, Chile, Volcán de Colima, Mexico and Vesuvius, Italy (e.g., Hagstrum and Champion 2002; Paterson et al. 2010). Additionally, although less common, some paleomagnetic studies were carried out to estimate emplacement temperatures of pyroclastic deposits from Santorini, Greece (e.g., McClelland and Druitt 1989; Bardot 2000; Tema et al. 2015) and from Vesuvius, Italy (e.g., Zanella et al. 2008; Di Vito et al. 2009).

Given the very recent ages of the lava flows, there are the only available techniques that can be used for dating.

In this work, rock-magnetic and paleomagnetic analyses were performed on lava flows and, for the first time, in pyroclastic material from the last big eruptions (*Lorenzo Pumice* and *Pink Pumice*) and ceramics embedded within these deposits of the NE section of the Popocatepetl volcano. We most mention, however, that the scarcity of accessible outcrops due to ~one thousand years of revegetation impedes a widespread sampling throughout the eruptive succession, while the expansion of agricultural activities and rural settlements the finding of archeological vestiges. Nevertheless, the obtained data have yield important preliminary results.

Geological framework

The trans-Mexican volcanic belt (TMVB) is a volcanic arc that crosses from east to west the central part of the Mexican territory. It is the result of the subduction of the Rivera and Cocos plates along the trenches of the Acapulco plate (Gómez-Tuena et al. 2005). It is usually divided into three sectors differentiated by their type of volcanism and its chemical composition: The west, central and east sectors (Ferrari 2000). The Popocatepetl volcano is part of the Sierra Nevada, located in the eastern sector of the TMVB; this sector is limited by the Taxco-Queretaro system and is characterized by containing large stratovolcanoes, calderas and complex domes of andesitic to rhyolitic composition.

Popocatepetl is a stratovolcano with a truncated crater made up of an alternation of andesitic and dacitic lava flows and pyroclastic deposits. In the last 5-ka BP, the volcano has presented three major Plinian eruptions: *Ochre Pumice* or Upper Pre-ceramic Plinian eruption (UPCPE, ~5000 year BP), *Lorenzo Pumice* or Lower Ceramic Plinian eruption (LCPE, ~2150 year BP) and *Pink Pumice* or Upper Ceramic Plinian eruption (UCPE, ~1100 year BP) (Siebe et al. 1996b). The three eruptions started with the emission of small amounts of ash and pyroclastic density currents. Subsequently occurred phreatomagmatic explosions, whose remaining flows spread radially at high speeds on the slopes of the volcano, which culminated in a paroxysmal phase with the emergence of a great Plinian column, pumice fall and the emplacement of pyroclastic density currents after the collapse of the column, ending with extensive lahars (Siebe et al. 1996a). Contemporaneously to the explosive eruptions, or at intermediate

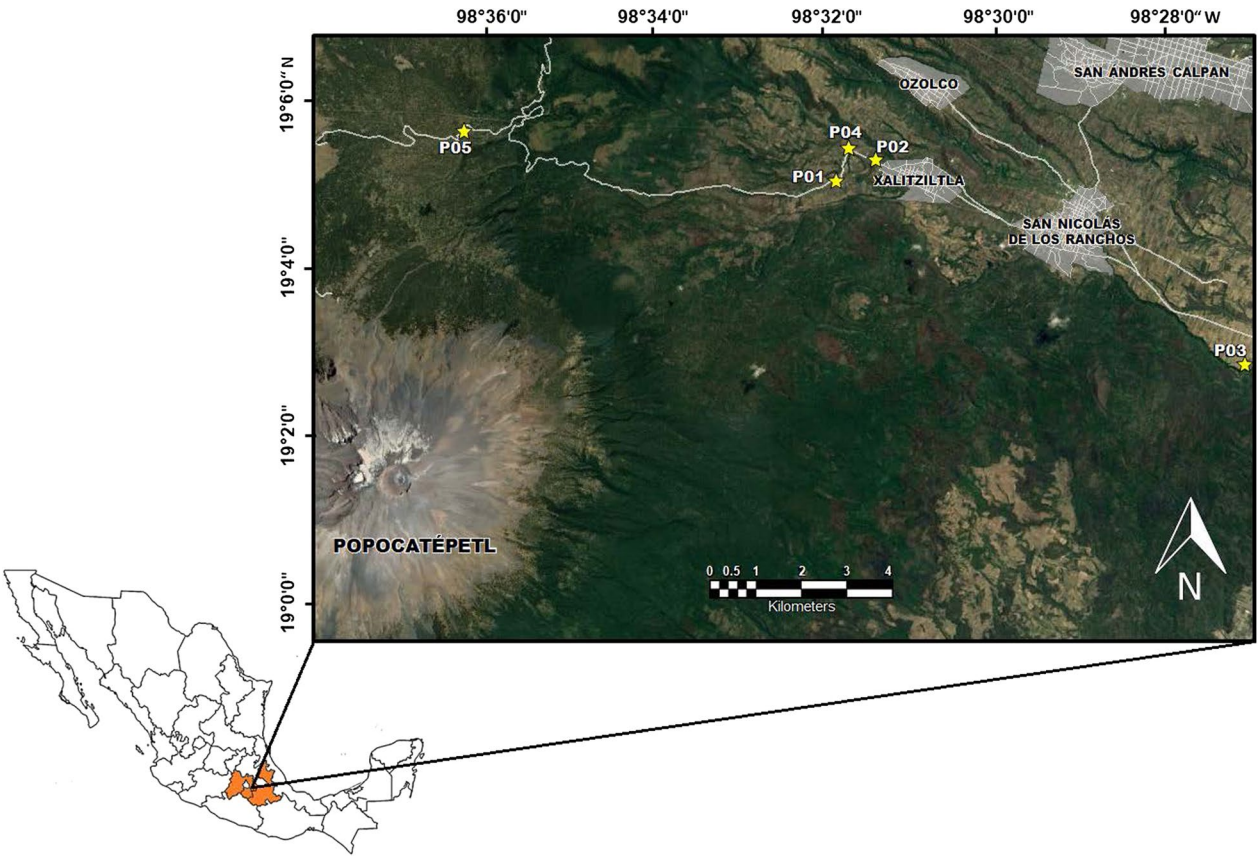

Fig. 1 Overview Google Earth image of the Popocatepetl volcano deposits/flows. Stars denote the location of the five paleomagnetic sites (PO-1–PO-5). Sites PO-1 and PO-2 correspond to pyroclastic density currents (Lorenzo and Pink Pumice, respectively), while PO-3 (Nealtican lava flow), PO-4 (Xalitzintla lava flow) and PO-5 (Buenavista dacite) correspond to lava flows. See text for details

stages, the Popocatepetl volcano has also presented effusive activity: Lava flows tapped through the central vent at the summit and fissural lava flows of andesitic composition (Schaaf et al. 2005).

Methodology

Field work

The three major Plinian eruptions were described at outcrops in the northeastern sector of the volcano, located at the towns of Buenavista, San Nicolás de los Ranchos, Santiago Xalitzintla, Tetimpa and Nealtican (Fig. 1), to obtain a composite stratigraphic column of the study area (Fig. 2). Paleomagnetic sampling of three lava flows and scoria clasts of two pyroclastic density currents (PDC) was carried out in field by using a water-cooled portable gasoline-powered rock coring drill. On average, eight standard one-inch paleomagnetic cores (6–12 cm long) were obtained for each lava flow (Buenavista dacite, Xalitzintla and Nealtican fissural lavas), which were distributed consistently both horizontally and vertically over the outcrops (Fig. 3).

Although the Xalitzintla—a light gray coloration lava (Fig. 3a)—and Nealtican—a darker coloration lava with reddish hues (Fig. 3b)—flows are thought to correspond to two eruptive pulses of the same event, since both are between the same volcano-sedimentary deposits but have different colors, we decided to sample both flows since they would log the same paleomagnetic record, and to check which one would be more suitable for paleomagnetic determinations.

Special care was dedicated to sampling only those blocks without evidence of post-emplacement dislodgment. We must note, however, that sampled outcrop at site PO-4 was already suspected to be tilted during field work, but since this was the best one that we could find at this flow, we decided, nonetheless, to give it a try.

In case of the two PDCs under the sequence of the *Pink Pumice* and *Lorenzo Pumice*, 20 paleomagnetic cores (8–12 cm long) were obtained by sampling five scoria clasts; nine cores from two clasts from the first sequence and 11 cores from three clasts from the second one (Fig. 4). This was possible due to the semi-consolidated

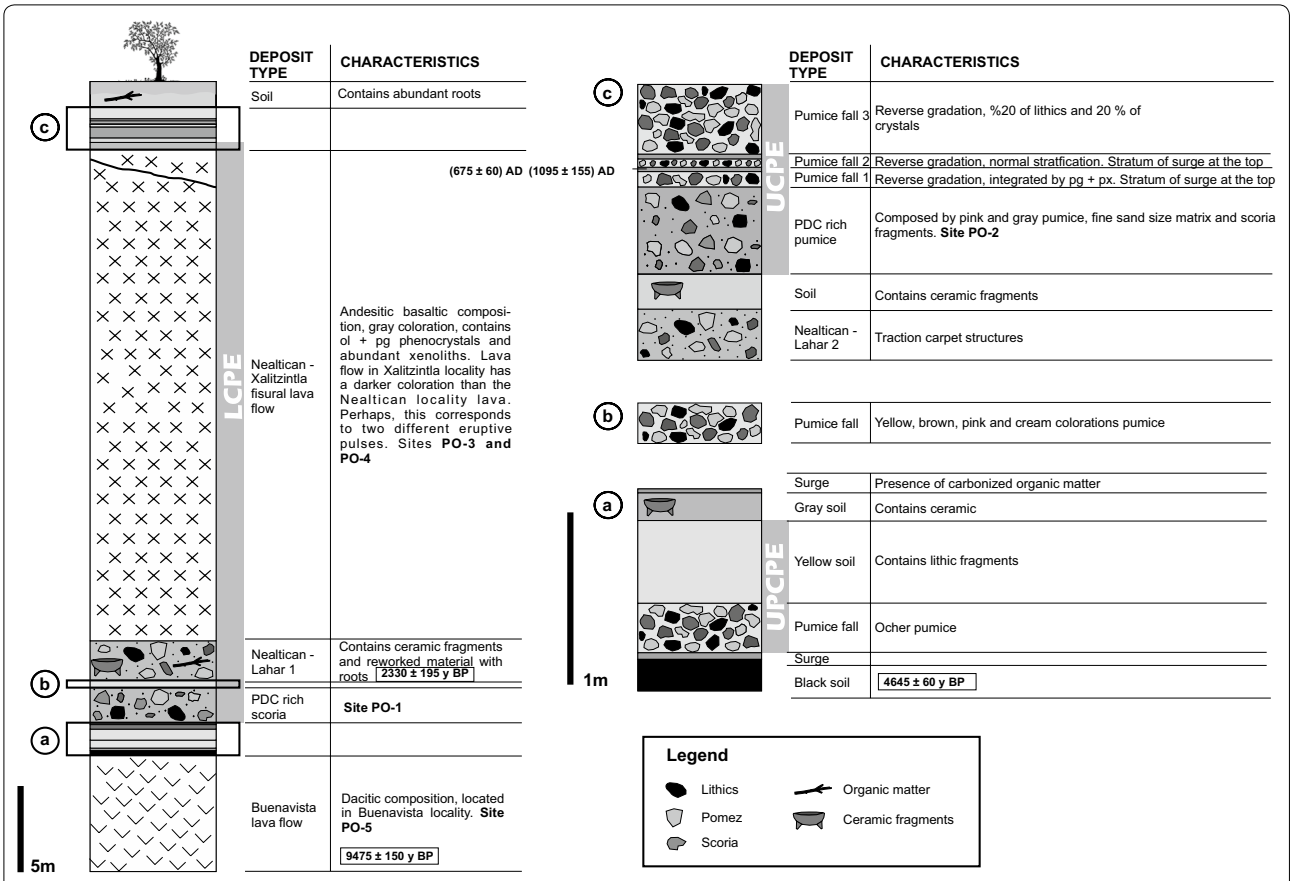

Fig. 2 Composite stratigraphic column of the study area. See text for details

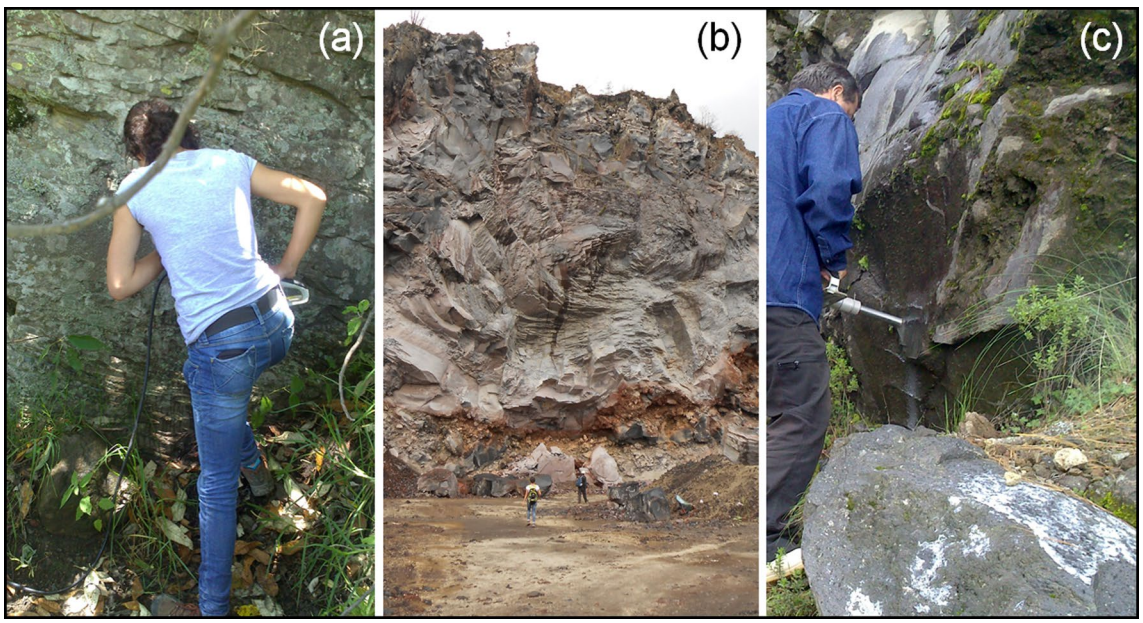

Fig. 3 Photographs of the different lava flows sampled. **a** Site PO-4, **b** site PO-3 and **c** site PO-5

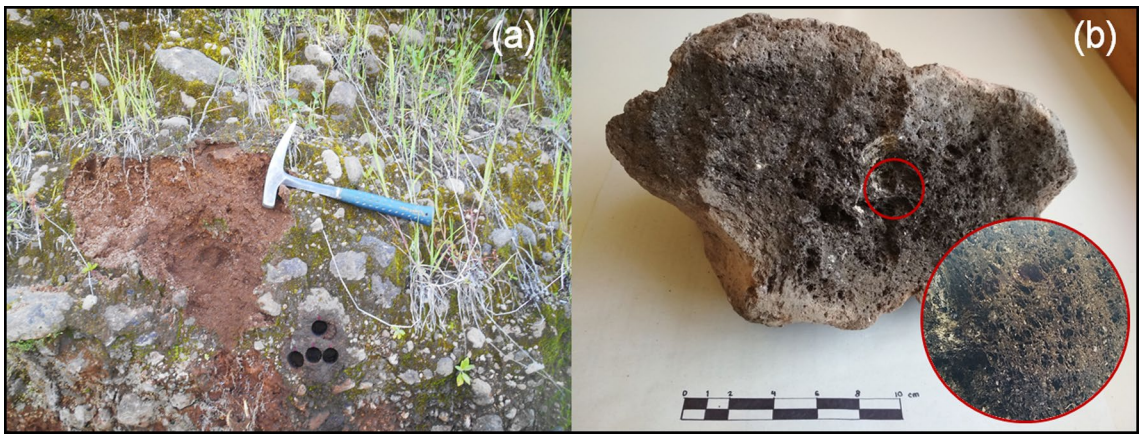

Fig. 4 **a** Photograph of the scoria clast (site PO-1). **b** View of a scoria clast

state of the PDCs. A total of 44 drilled cores were obtained. Measurement of the azimuth and dip of in-place cores was carried out by means of a precision core orienting fixture, with coupled magnetic compass. Paired sun-compass orientation was carried out when possible.

Also, eight ceramic fragments—1–5 cm long—(Fig. 5a) were collected from a reworked floor of pink tones at the top of the recorded stratigraphic sequence, below the eruptive UCPE. The whole sequence covering the stratum from which the ceramics were obtained has a thickness of approximately 1.5 m (Fig. 5b). Based on the color and type of material of the different ceramic shards, these could belong to the same ceramic style. Nine ceramic fragments of varying sizes—between 2 and 7 cm long—(Fig. 5c) were unearthed from a gray colored soil at the base of the LCPE eruptive sequence, approximately 60 cm from the surface, which were covered by a pyroclastic density current and an agricultural soil (Fig. 5d). Differences in the color of the fragments can be observed; thus, they probably correspond to different ceramic artifacts.

Although in the first case it was not possible to recognize what kind of vase the shards come from due to their small and irregular shape, in the second one some of the shards likely come from an ornamental tripod vase. In both cases, however, the shards should come from a simple (rough) manufacturing process.

Laboratory procedures

Drilled cores were divided into two or more standard cylindrical paleomagnetic samples (1-inch diameter × 1-inch height), obtaining a total of 65 specimens. The bigger pottery shards recovered from both pumice sequences were additionally broken into at least 6 specimens. These specimens, together with the smaller shards, were pressed into salt pellets to treat them as standard paleomagnetic specimens, obtaining 47 archeomagnetic specimens in total, which were dedicated to rock-magnetic experiments, archeointensity (AI) determinations, and to investigate emplacement temperatures of the pyroclastic flows. See below for details.

Bulk magnetic susceptibility (k) measurements were obtained by means of a Bartington MS2B dual-frequency sensor attached to a Bartington MS2 susceptibility meter. Rock-magnetic experiments were performed in air, using a variable field translation balance (AVFTB) from Magnetic Measurements Ltd, to identify the magnetic mineralogy (remanence carriers) and their thermal stability, and to investigate the suitability of the material (lavas and scoria) to obtain reliable paleointensity (PI) determinations. These experiments included: (1) isothermal remanence magnetization (IRM) acquisition curves, (2) hysteresis loops, (3) backfield curves and (4) thermomagnetic curves. Saturation remanent magnetizations (M_{rs}), saturation magnetizations (M_s) and coercivity fields (B_c) were retrieved after correction for paramagnetic contribution of hysteresis cycles with applied fields up to ± 0.7 T. Coercivities of remanence (B_{cr}) were determined by applying progressively increasing backfields after saturation. Thermomagnetic curves were obtained between room temperature and 600 °C. Detailed tumbling stepwise alternating field (AF) demagnetization up to 100 mT (using an AGICO LDA 3 equipment) and thermal demagnetization (using an ASC Scientific TD48 furnace) up to 600 °C of samples were performed to isolate the characteristic remanent magnetization (ChRM) of the samples from the three lava flows and from clast of the scoria flows. Natural remanent magnetization (NRM) and laboratory induced magnetizations (TRMs) were

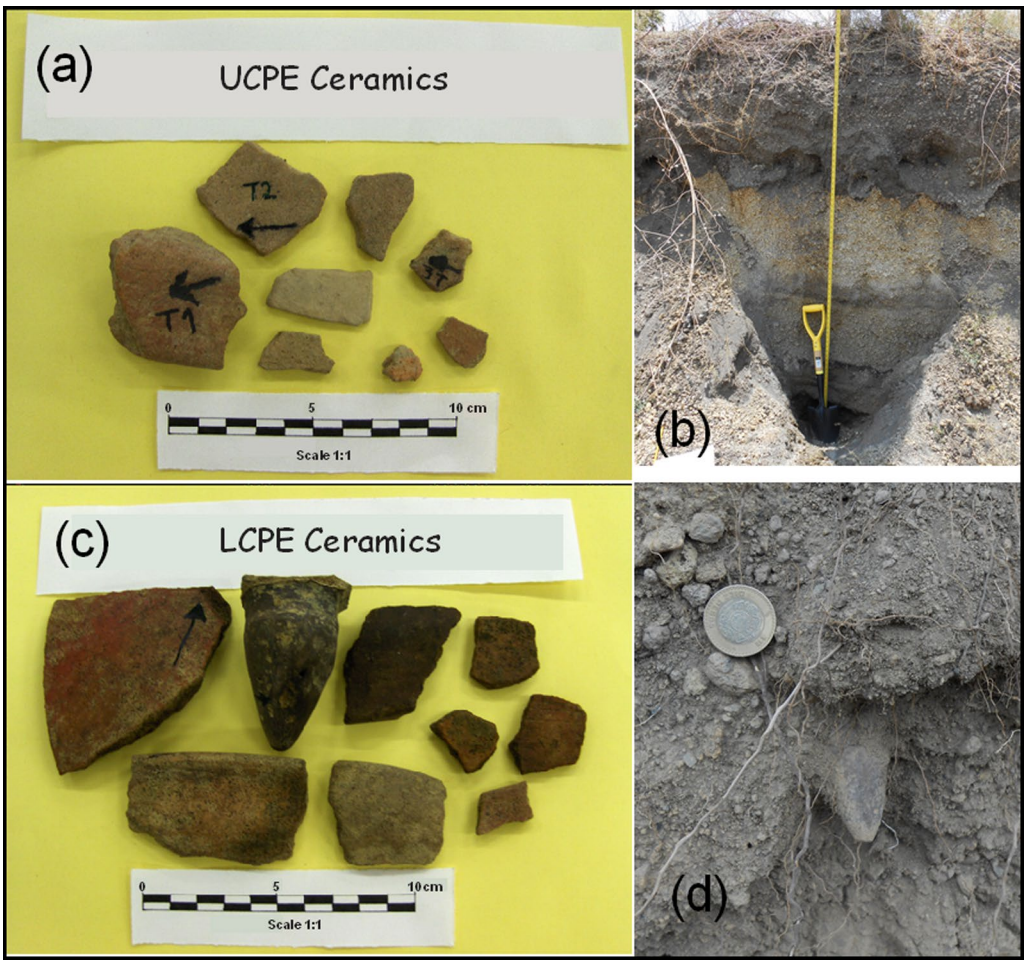

Fig. 5 Different ceramic shards studied. **a** Ceramic shards buried from the UCPE pyroclastic density current. **b** View of the UCPE pyroclastic density current. **c** Ceramic shards buried from the LCPE pyroclastic density current. **d** View of the LCPE pyroclastic density current

measured in all cases by means of an AGICO dual speed JR6 spinner magnetometer.

Specimens were subjected to the Thellier–Coe (TC) method of paleointensity (PI) determinations (Thellier and Thellier 1959; Coe 1967) at Laboratorio Interinstitucional de Magnetismo Natural (LIMNA) facilities. The experiments were carried out using a ASC Scientific TD48-SC furnace; all heating/cooling steps were performed in air. Ten temperature steps were distributed through the entire temperature range (from room temperature to 560 °C) with reproducibility better than 2 °C between two heating steps. The laboratory field strength was set to (45.0 ± 0.5) μT along the cylindrical axis of the paleomagnetic cores. Partial thermoremanent magnetization (pTRM) checks, carried out every third temperature step, as well as pTRM tail checks determinations (Riisager and Riisager 2001) at 350 °C and magnetic susceptibility measurements of lava specimens and ceramic shards after each double heating-step were also added to the protocol.

As stated by Chauvin et al. (2000), archeomagnetic objects that have an anisotropic shape, such as tiles and bricks, are often characterized by a strong magnetic anisotropy. Such anisotropic shape deviates the direction of the TRM acquired by these objects during initial cooling from the local direction of the geomagnetic field (e.g., Tema 2009), while their TRM intensity depends on the direction in which the local field is applied. In order compensate the AI determinations on the ceramic shard investigated we followed the adjustment technique described by Selkin et al. (2000), which requires the measurement of the remanence anisotropy tensor χ_{ARM}. At the end of the Thellier–Coe experiments, the specimens were given an ARM (180 mT AC field; 0.30 mT DC field) along 6 axial directions ($\pm X$, $\pm Y$ and $\pm Z$)—using an LDA 5 AF demagnetizer coupled to

a PAM 1 anhysteretic/pulse magnetizer from AGICO—following the C-mode protocol described in the ARM—Brief Practical Guide Application note (AGICO Prints 2018). Between each ARM step, an AF demagnetization at 200 mT was performed to be used as a baseline. The remanence anisotropy tensor χ_{ARM} was determined using the Anisoft5 software (Anisoft5 2018). Finally, the anisotropy correction factors (f_{ARM}) were estimated—as the ratio between the remanence acquired in a unit field parallel to the ancient field and the remanence acquired in a unit field in the laboratory field direction—and the AI values corrected.

Aimed to quantifying the cooling rate (CR) effect in our samples, the CR dependence of TRM was investigated applying a modified protocol to that described by Chauvin et al. (2000). At the end of the AI experiments, all specimens were heated two more times at the highest temperate reached during the AI experiment (560 °C) under the same laboratory field used during it. Last measurement (in field step) of the AI experiment was designated as TRM_1. Then, a second TRM (TRM_2) was induced to all the samples, but using this time a longer cooling time (~6 h). Lastly, a third TRM (TRM_3) was created using the same cooling time as that used during the TRM_1 creation (~45 min). The cooling rate factor f_{CR} was calculated as the ratio between the intensity acquired during a long and a short cooling time: $f_{CR} = TRM_2/TRM_1$. Changes in TRM acquisition capacity were estimated by means of the percentage variation between the intensity acquired during the same cooling time ($f_{AC} = TRM_3/TRM_1$). The cooling rate correction was only applied when the corresponding change in TRM acquisition capacity was close to 1 and $f_{CR} > 1$ (Morales et al. 2009).

Emplacement temperature estimation of PDCs relies on the identification of two components of magnetization within the "accidental scoria clasts" (clasts of the existing volcanic structure): the original, higher temperature component, which will be randomly oriented for an assemblage of clasts, and a lower temperature component that will consistently align with the Earth's magnetic field at the time of emplacement (Paterson et al. 2010). The highest temperature at which the low-temperature component is still present provides an estimate of the emplacement temperature of the clast during a conventional stepwise thermal demagnetization process.

Results

Rock-magnetic experiments

NRM intensity versus magnetic susceptibility variation for the three studied lavas and scoria clasts, together with lines of constant Königsberger's ratio (Q), is shown in Fig. 6. Most samples lie between lines with $1 < Q < 10$, while some few others between lines with $10 < Q < 100$—mainly those of site PO-05—. As will be discussed later, acquisition of strong (secondary) isothermal remanence magnetizations (IRMs)—evidenced by high Q ratios—could impede to retrieving the characteristic (original) remanent magnetization (ChRM) acquired during cooling of the lava.

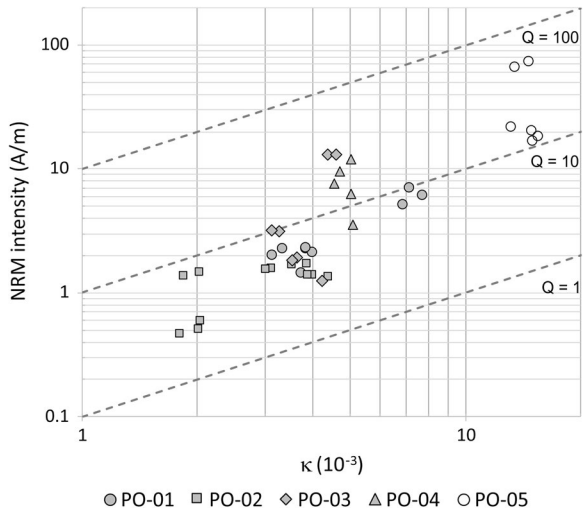

Fig. 6 Variation of the NRM intensity and magnetic susceptibility for the three studied lavas and scoria clast, together with lines of constant ratio ($Q = NRM/\kappa \cdot H$); the ratio between remanent and induced magnetizations, where κ is the initial magnetic susceptibility and $H = 33$ Am^{-1} the magnetic field intensity

Results from isothermal remanence magnetization (IRM) acquisition curves show that all volcanic samples, except those from the Xalitzintla lava flow (site PO-4), got saturation at fields between 200 and 250 mT, which suggest the dominance of low coercivity (titano-) magnetite minerals of pseudo-single-domain (PSD) grain size. Those from site PO-4 did it at fields up to 500 mT, suggesting the presence of hematite (upper part of Fig. 7). Ceramic samples got saturation also at fields above 300 mT, pointing to the dominance of medium coercivity (titanomagnetite) minerals of single-domain (SD) and/or PSD grain size (lower part of Fig. 7), which is considered as a suitable magnetic mineralogy for paleointensity (PI) determinations.

Estimation of the domain state (grain size) of the magnetic mineralogy is of fundamental importance since only non-interacting SD grains follow the laws of partial thermoremanences (pTRMs) of Thellier (Thellier and Thellier 1959), on which the Thellier-type experiments are based (see Dunlop 2011 for a review). On the other hand, the shape—pot-bellied or wasp-waisted—of a hysteresis curve yields also an insight of the composition—single or multiple magnetic phases—of the rock sample. Hysteresis curves for volcanic materials present both pot-bellied (site PO-1 and site PO-3) and wasp-waisted (site PO-2,

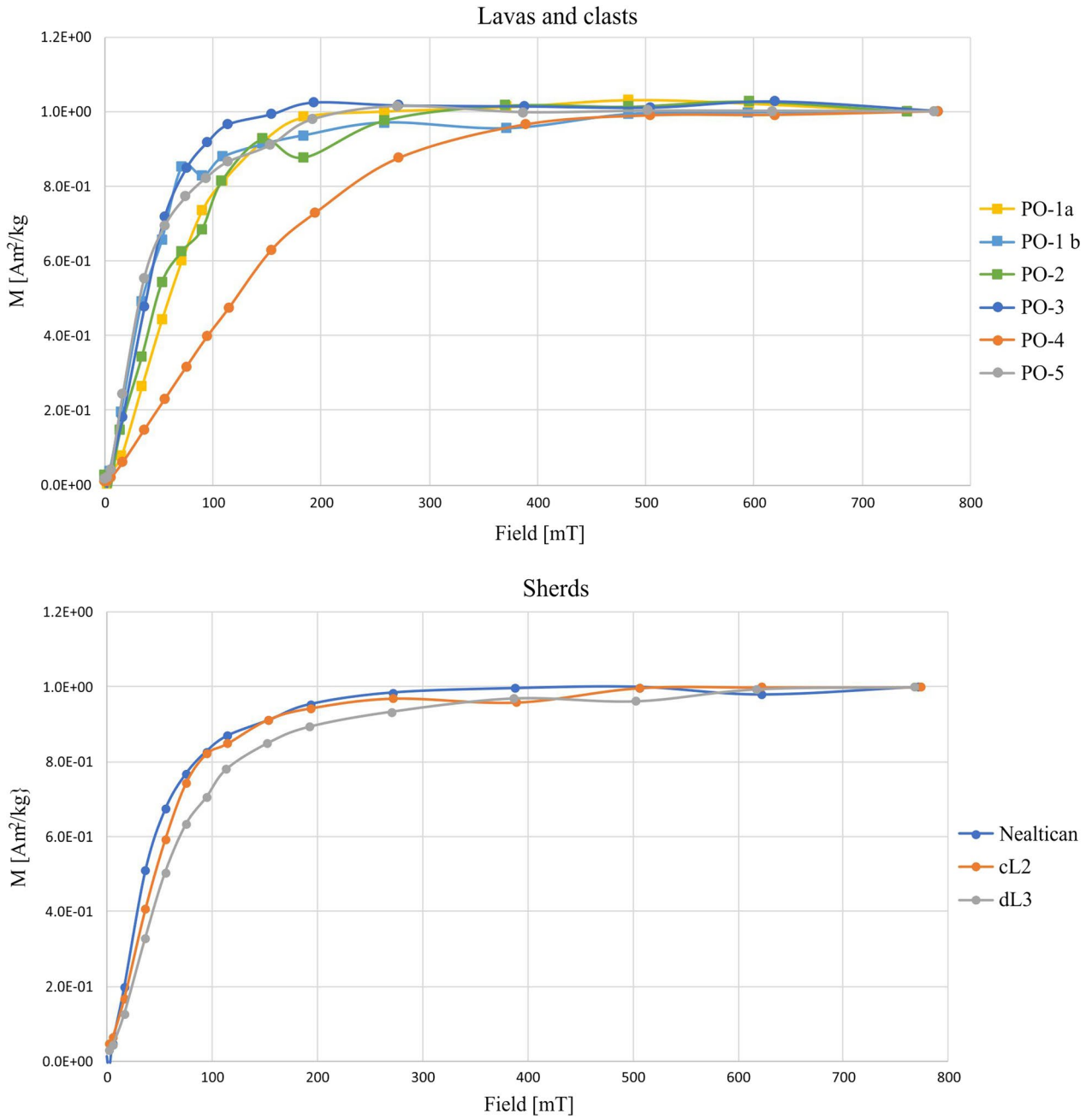

Fig. 7 Representative examples of isothermal remanent magnetization (IRM) acquisition curves for the three lava flows and scoria clast sampled (upper plots) and three ceramic fragments (lower plots)

site PO-4 and site PO-5) shapes, with different values of paramagnetic contribution (Fig. 8). Saturation magnetization M_s of (3.1, 2.4, 4.1 and 7.1) $\times 10^{-4}$ Am^2 kg^{-1} was obtained for these samples from sites PO-1, PO-3, PO-4 and PO-5, respectively, with coercive force B_c values of (8.7, 13.0, 5.16 and 15.1) mT. Remanent saturation magnetization M_{rs} values are quite similar for the samples from sites PO-1, PO-3 and PO-4 (3.7, 4.0 and 3.3) $\times 10^{-5}$ Am^2 kg^{-1}, while that for site PO-5 reaches up to 1.9×10^{-4} Am^2 kg^{-1}. Site PO-2, on the contrary, presents the lowest values of M_s (9.0×10^{-5} Am^2 kg^{-1}) and M_{rs} (8.4×10^{-6} Am^2 kg^{-1}). Magnetization ratios M_{rs}/M_s versus coercivity ratios B_{cr}/B_c are displayed in a Day plot (Day et al. 1977). While lava samples plot mainly in the

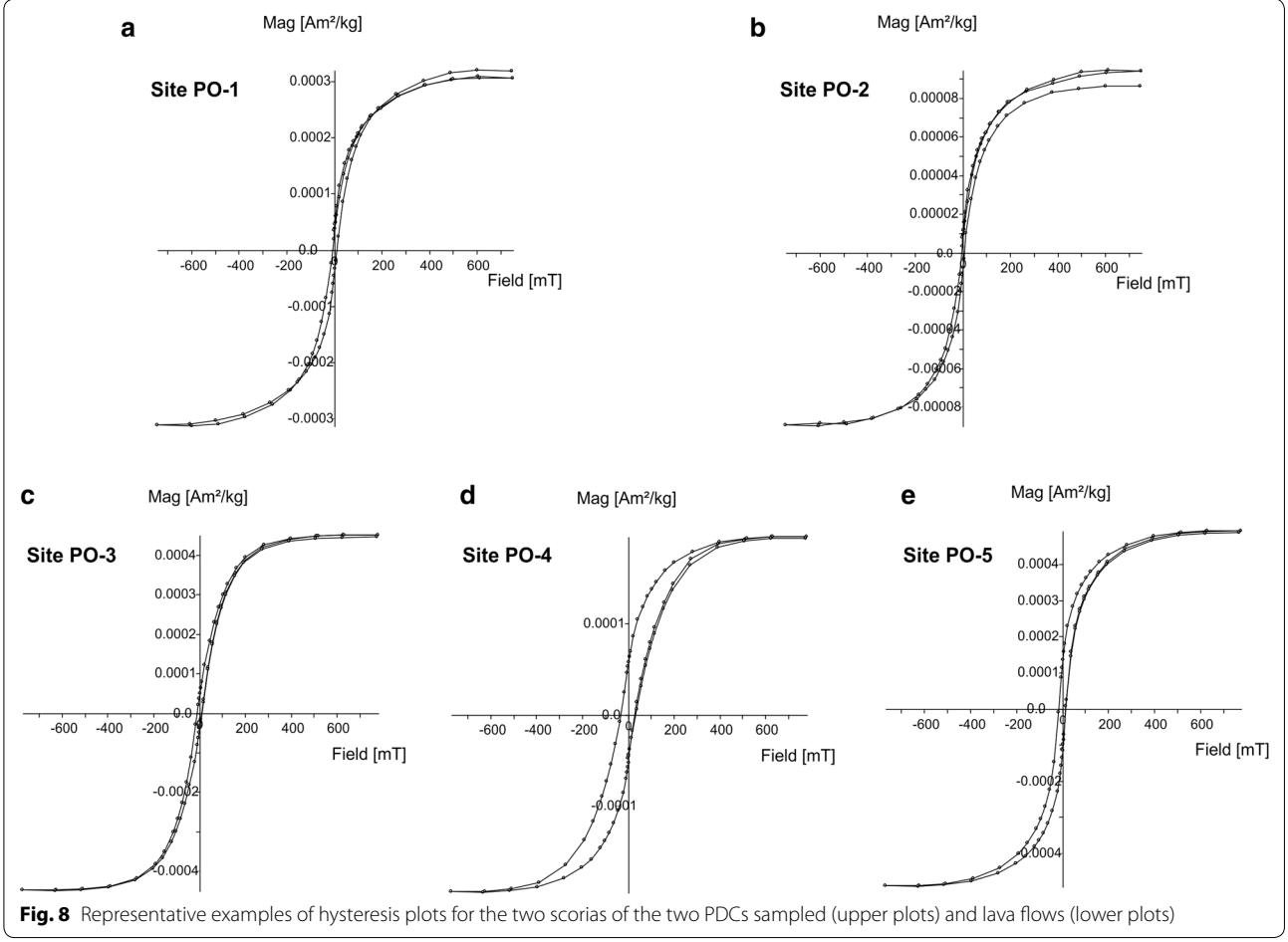

Fig. 8 Representative examples of hysteresis plots for the two scorias of the two PDCs sampled (upper plots) and lava flows (lower plots)

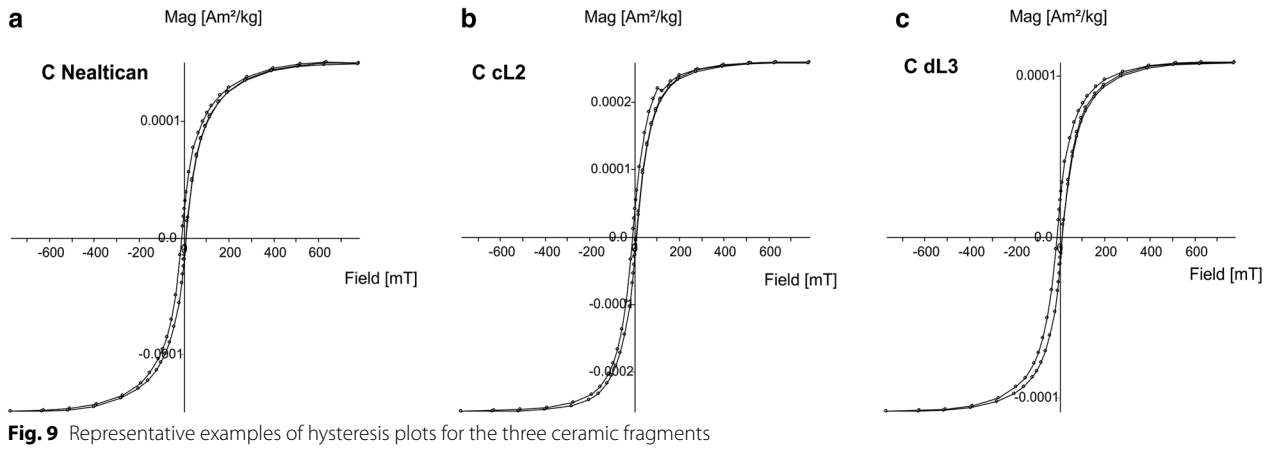

Fig. 9 Representative examples of hysteresis plots for the three ceramic fragments

PSD region, scoria clasts show a tendency toward multi-domain (MD) grain size (Fig. 10a). However, it is worth mentioning that Day plots are not a very reliable means of determining domain structure.

In the case of the ceramic samples, all magnetic parameters retrieved from the rock-magnetic experiments (AVFTB), and their corresponding ratios, are quite similar for three representative pottery shards (on average, $B_c = 9$ mT; $B_{cr} = 40$ mT; $M_s = 1.7\ 10^{-4}$ Am^2 kg^{-1}; $M_{rs} = 2.3$

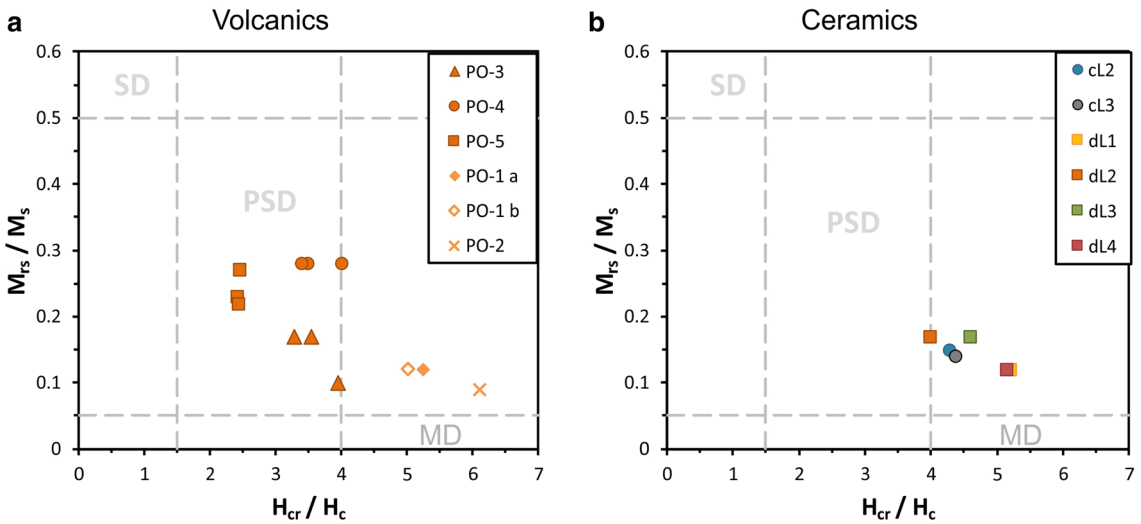

Fig. 10 Corresponding Day plot (M_{rs} saturation remanence, M_s saturation magnetization, B_{cr} remanence of coercivity, B_c coercive force) for the lava flows, scoria clast (**a**) and ceramic fragments (**b**)

10^{-5} Am^2 kg^{-1}; $M_{rs}/M_s = 0.14$; and $B_{cr}/B_c = 4.6$) (Figs. 9, 10b). Although ceramic samples show a tendency toward MD grain size, again, day plots are not a very reliable mean of determining domain structure.

Thellier-type experiments are basically an in-laboratory stepwise recreation of the process that led origin (in nature) to the (thermo-) remanent magnetization acquired by a volcanic rock during cooling. As so, this stepwise recreation requires a multiheating process at increasing temperatures up to the Curie temperature of the magnetic mineralogy of the volcanic material, which could alter it giving raise to the creation of (secondary) chemical magnetizations. A qualitative—but also quantitative—way of estimating the degree of alteration experienced by a sample due to heating is provided by the reversibility of the M–T curves. Temperature variation of magnetization (M–T curve) for the PDC PO-1 presents a markedly decrease at a temperature below 100 °C. After this temperature, it gradually increases up to ~350 °C (Fig. 11a). Continuous decrease till 600 °C does not allow a clear identification of the Curie temperature (T_c) of the mineral phase responsible for the magnetization. Cooling branch closely follows that of the heating one up to ~450 °C; after that, it departs of the heating one. Nonetheless, the very low temperature phase (~100 °C) appears again during cooling. On the contrary, corresponding M–T curve for the PDC PO-2 presents a markedly decrease up to a temperature below 300 °C, after which gradually deceases till 600 °C (Fig. 11b). Three different T_c can be identify: 330 °C, 490 °C and 574 °C, the last one corresponding to very low Ti titanomagnetite.

M–T curves for the Nealtican and Xalitzintla lavas are highly reversible (Fig. 11c, d), while that corresponding to the Buenavista lava is rather irreversible (Fig. 11e). However, we note that from this experiment it cannot be ascertained at which temperature started the alteration. Results of thermomagnetic experiments—analyzed using the RockMagAnalyzer 1.0 software (Leonhardt 2006)—indicate the presence of one, two and up to four minerals phases, with quite variable Curie temperatures (T_c), for the Nealtican, Xalitzintla and Buenavista lavas, respectively (Fig. 11c–e). The mineral phase for the Nealtican lava shows a T_c ~520 °C. Corresponding mineral phases for the Xalitzintla lava show T_c's of ~400 and 540 °C. Buenavista lava, on the contrary, show minerals phases with T_c of ~160, 270, 360 and 560 °C. These T_c spectra suggest the coexistence of Ti–rich and Ti-poor titanomagnetite minerals, as well as the probably presence of maghemite (T_c ~300 °C).

In the case of the ceramics, corresponding thermomagnetic curves are highly reversible (Fig. 12b, c), except that coming from Nealtican, which is somewhat irreversible (Fig. 12a). All curves show the presence of two to three magnetic phases: the lower one with T_c ~200 °C, the intermediate with T_c between 350 and 470 °C, while the third one with T_c around 500–560 °C (Fig. 12a–c).

Paleodirection and paleointensity determinations

While paleodirection is normally parallel to that of the magnetizing Earth's field—and is measured directly using a magnetometer—paleointensity is only proportional to the field strength of the Earth's field present during cooling and its determination is an indirect estimation. However, during their geological past—and also in laboratory

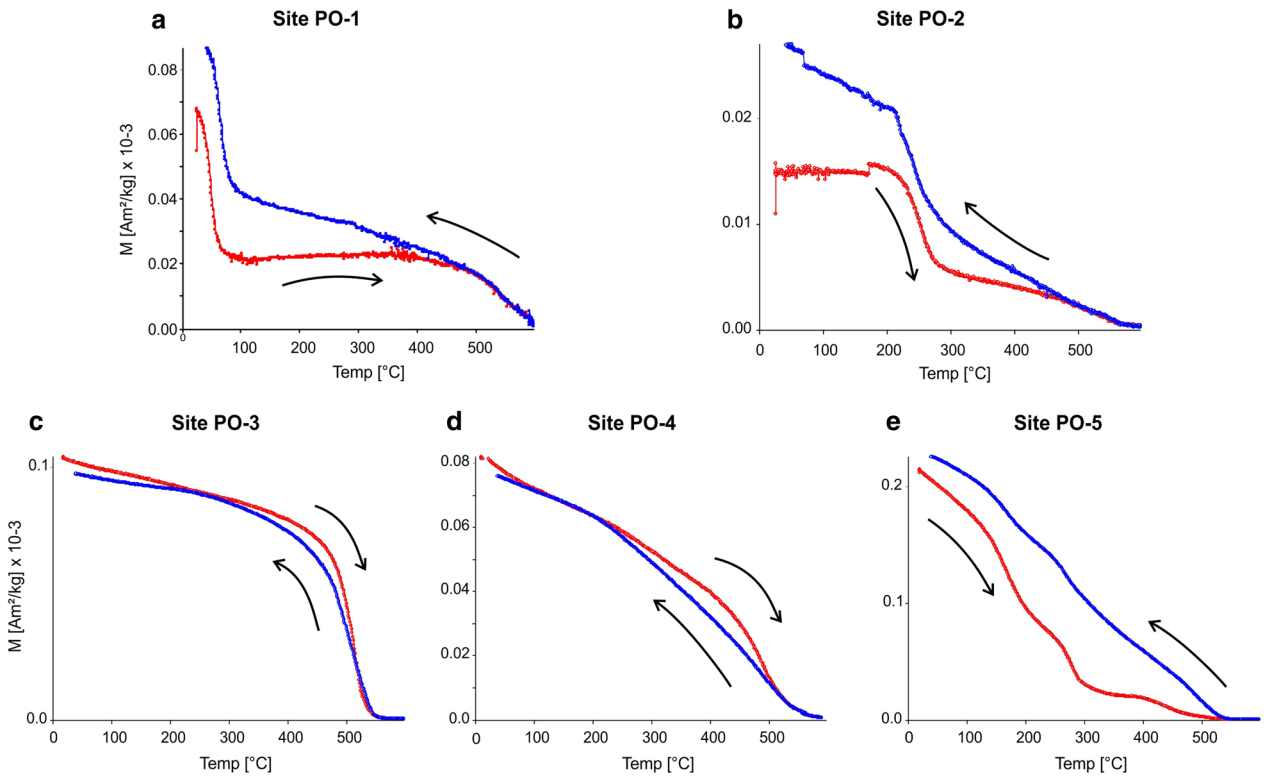

Fig. 11 High-field-induced magnetization versus temperature (M–T) plots for the two scorias of the two PDCs (**a**, **b**) and the three lavas (**c**–**e**)

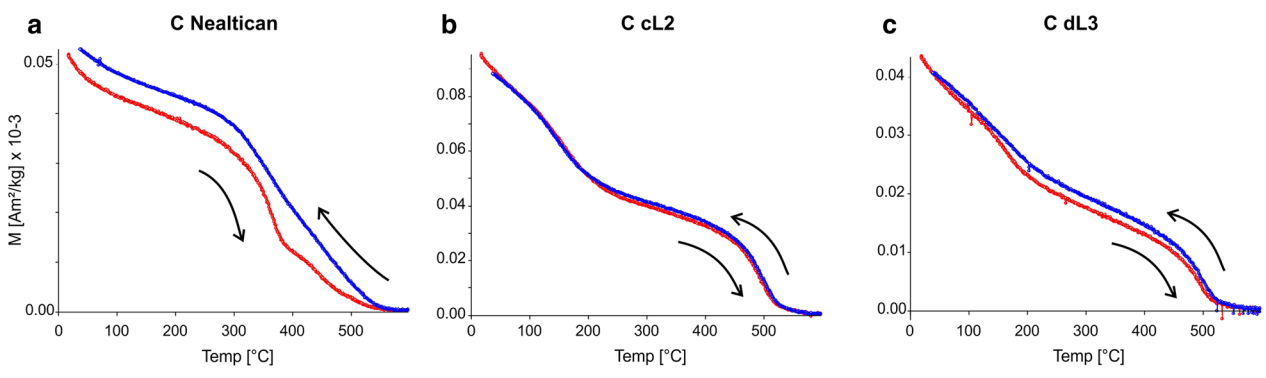

Fig. 12 High-field-induced magnetization versus temperature (M–T) plots for the three ceramic fragments (**a**–**c**) studied from Popocatepetl

and during the course of the experiments—volcanic rocks are prone to the acquisition of secondary magnetizations that can mask the (original) characteristic remanent magnetization (ChRM). Therefore, the isolation of the ChRM by means of alternating field (AF) or thermal demagnetization processes is required.

Stepwise demagnetization and paleodirections

Pilot specimens, representative of the different samples under study (lavas, scoria clast and ceramic shards), were selected for both alternating field (AF) and thermal demagnetization experiments. Site-mean directions were investigated using the Remasoft 3.0 software (Chadima and Hrouda 2006).

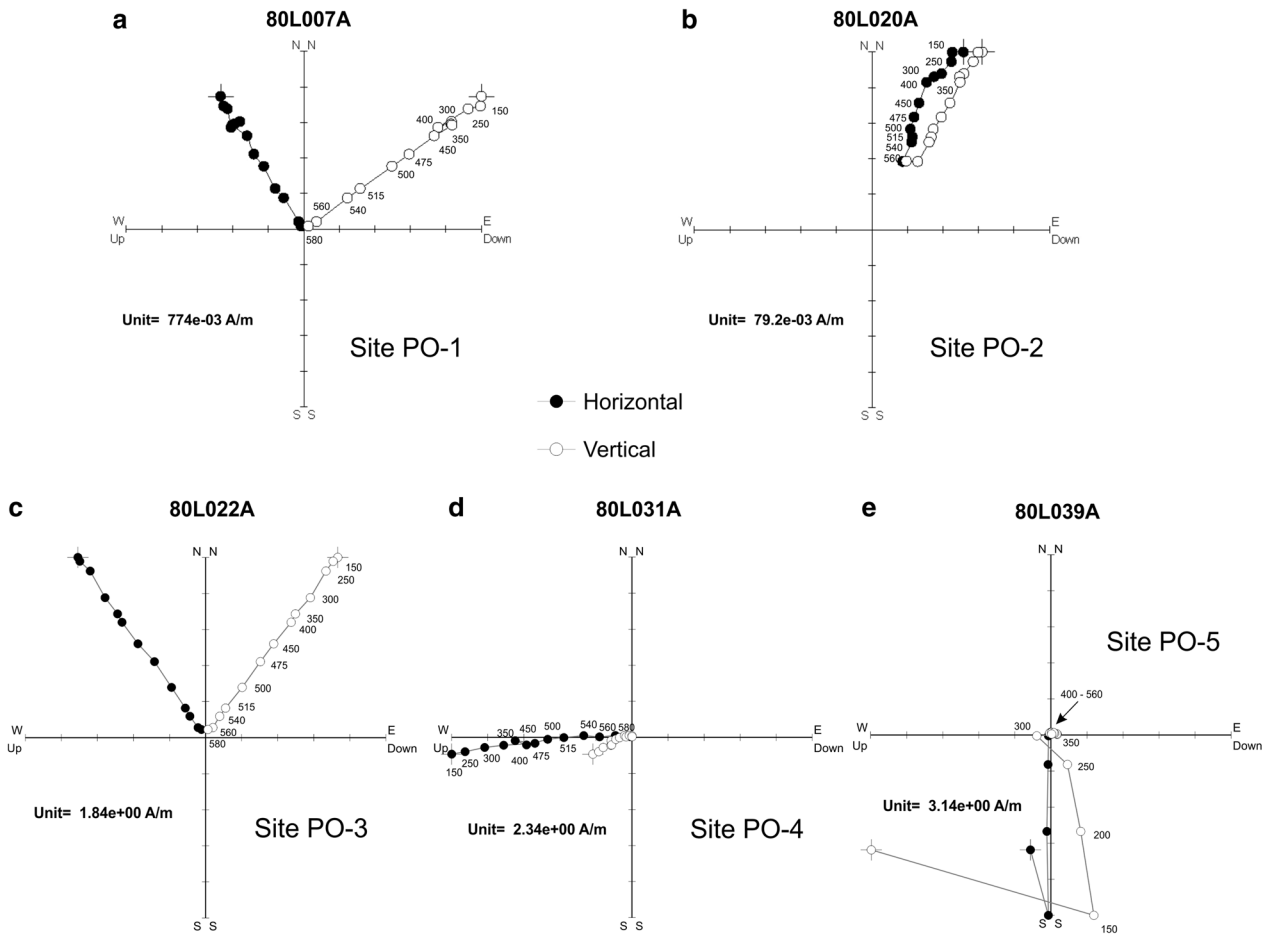

Fig. 13 Representative normalized orthogonal vector plots (Zijderveld diagrams) of stepwise thermally demagnetized samples from **a** site PO-1, **b** site PO-2, **c** site PO-3, **d** site PO-4 and **e** site PO-5. Labels along horizontal curves denote the temperature during the demagnetization step. See text for more details

Pyroclastic density currents

Specimens of site PO-1 displayed mainly a single paleomagnetic component directed through the origin, accompanied by an initial weak overprint of possibly viscous origin (Fig. 13a) which could be removed at fields/temperatures below 10 mT/150 °C. On the contrary, those from site PO-2 presented a composite-trace Zijderveld diagram, with at least two components which were not fully demagnetized at 580 °C (Fig. 13b). Attempts to retrieving mean direction from the PDCs (sites PO-1 and PO-2) yielded a mean direction (Dec = 337.3°, Inc = 49.2°, $\alpha_{95} = 4.5°$) for the first PDC, and a three clusters plot with well-differentiated directions for each cluster for the second PDC (Fig. 14a, b, respectively).

Lava flows

Most of the specimens of site PO-3 displayed mainly a single paleomagnetic component, occasionally accompanied by an initial weak overprint of possibly viscous origin (Fig. 13c), which could be removed at fields/temperatures below 10 mT/150 °C. Nonetheless, it was possible to obtain a stable end direction in such cases, comparable to those specimens unaffected by such overprints. Corresponding mean direction (Dec = 338.9°, Inc = 32.2°, $\alpha_{95} = 6.4°$) is shown in Fig. 14c. Although specimens from site PO-4 also displayed mainly a single paleomagnetic component (Fig. 13d), an anomalous mean direction (Dec = 267.7°, Inc = −5.0°, $\alpha_{95} = 6.8°$) was obtained (Fig. 14d). In the case of site PO-5 most of the specimens displayed some strong secondary components—likely of viscous (VRM) and/or isothermal origin (IRM)—and erratic directions throughout the thermal demagnetization process were obtained (Fig. 13e). They were, nonetheless, able to be removed at fields/temperatures below 10 mT/150 °C. As a result of their presence, a quite scattered mean direction was obtained (Fig. 14e). Table 1 displays the mean ChRM directions obtained for the three lava flows and two PDCs studied.

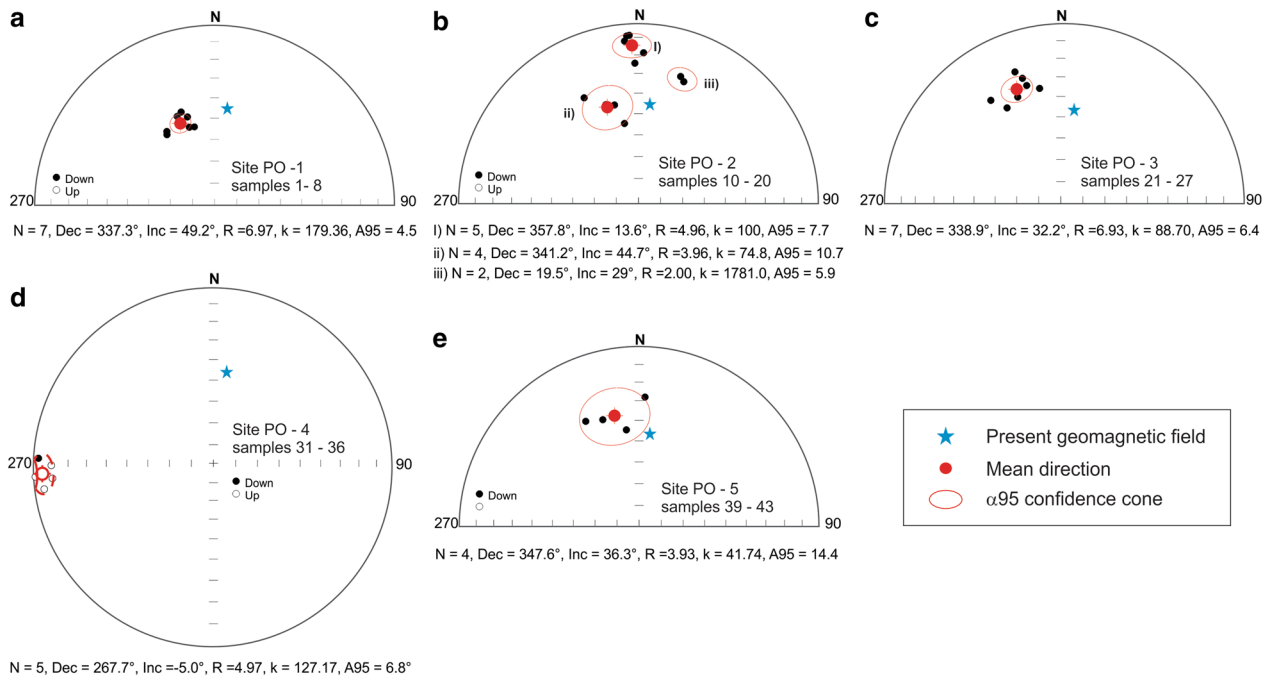

Fig. 14 Stereo plots showing the characteristic remanent magnetization (ChRM) directions for the studied pyroclastic density currents (**a** and **b**) and lava flows (**c**–**e**). Flow mean directions are shown by the red dots, together with their corresponding 95% confidence angles

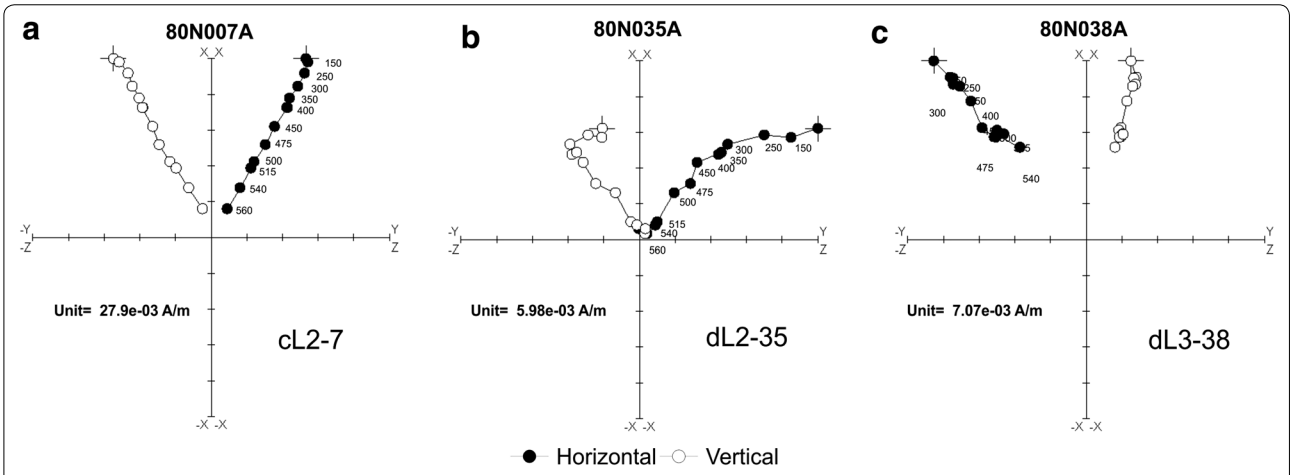

Fig. 15 Representative normalized orthogonal vector plots (Zijderveld diagrams) of stepwise thermally demagnetized samples from **a** ceramic sherd cL2, **b** ceramic sherd dL2 and **c** ceramic sherd dL3. Labels along horizontal curves denote the temperature during the demagnetization step. See text for more details

Ceramics

Ceramic sherd labeled cL2 displayed also a single paleomagnetic component, infrequently accompanied by an initial weak overprint of possibly viscous origin (Fig. 15a), which could be removed at fields/temperatures below 10 mT/150 °C. Ceramic sherd labeled dL2 presented clearly a stronger secondary component, removed at 300–350 °C. Nonetheless, its primary component is directed toward the origin (Fig. 15b). Finally, ceramic sherd labeled dL3 showed a behavior alike that of dL2, although its NRM reduced only to almost 50% at 560 °C (Fig. 15c).

Table 1 Site-mean directions for the Popocatepetl paleomagnetic sites, with sampling coordinates

Site	Field code	Latitude	Longitude	*N*/*n*	*R*	*k*	α_{95}	Dec (°)	Inc (°)
Xalitzintla	PO-1* (I)	19°04′55.15″	98°31′55.50″	3/2	2.0	210.6	17.3	343.4	47.9
Xalitzintla	PO-1* (II)	19°04′55.15″	98°31′55.50″	6/5	4.98	188.2	5.6	335.1	49.4
Xalitzintla	PO-2* (I)	19°05′02.28″	98°31′28.74″	5/5	4.96	100.0	7.7	357.8	13.6
Xalitzintla	PO-2* (II)	19°05′02.28″	98°31′28.74″	4/4	3.96	74.80	10.7	341.2	44.7
Xalitzintla	PO-2* (III)	19°05′02.28″	98°31′28.74″	2/2	2.00	1781.0	5.9	19.5	29.0
Nealtican	PO-3	19°02′42.18″	98°26′46.50″	7/7	6.93	88.70	6.4	338.9	32.2
Xalitzintla	PO-4	19°05′10.38″	98°31′50.46″	8/5	4.97	127.17	6.8	267.7	−5.0
Buenavista	PO-5	19°05′21.30″	98°36′37.50″	8/4	3.93	41.74	14.4	347.6	36.3

Sites with an asterisk denote pyroclastic density current (PDC)

N number of recovered drill cores, *n* number of specimens used for the calculation of site-mean direction, *R* unit vector sum, *k* precision parameter, α_{95} 95 per cent confidence level, Dec declination, Inc inclination

Table 2 Thellier–Coe paleointensity results for site PO-3 (Neáltican lava flow)

Specimen	ΔT (°C)	*N*	β	*f*	*g*	*q*	δ(CK)	δ(TR)	MAD_{anc}	Class	H_{raw} (μT)	$\pm\sigma H$ (μT)	*f*	H_{crc} (μT)
21A	150–560	11	0.04	0.59	0.86	12.2	5.9	3.3	2.1	B	55.4	2.29	1.11	49.9
22A	200–560	10	0.03	0.90	0.87	30.0	2.7	7.7	0.9	B	59.7	1.55	1.08	55.2
23B	200–560	10	0.02	0.91	0.87	32.4	5.1	7.0	1.1	B	59.5	1.46	1.02	58.3
24C	200–560	10	0.06	0.71	0.77	9.3	6.4	7.0	1.1	B	61.8	3.61	1.03	60.0
25A	250–560	9	0.05	0.76	0.78	12.5	0.3	7.8	1.5	A	63.6	3.04	1.04	61.2
26B	250–560	8	0.04	0.69	0.83	15.7	7.9	4.4	1.5	B	60.8	2.24	1.04	58.4
27A	250–560	9	0.03	0.75	0.85	23.5	6.5	4.1	1.2	B	61.6	1.65	1.05	58.6
									Mean =		60.3			57.4
									1σ =		2.6			3.8

δT temperature interval used for the intensity determination, *N* number of heating steps used for the intensity determination, $\beta = \sigma m/m$ (*m* slope of the best fit line, σm standard deviation of *m*), *f* fraction of extrapolated NRM used for intensity determination, *g* gap factor, *q* quality factor as defined by Coe et al. (1978), δ(CK), δ(TR), MAD_{anc} and class as defined by Leonhardt et al. (2004), H_{raw} raw archeointensity value, σH standard deviation of *H*, *f* cooling rate correction factor, H_{crc} cooling rate-corrected archeointensity

Paleointensities

In spite of the non-promising rock-magnetic results of site PO-5 lava flow and Nealtican ceramic sherds for PI experiments, we decided to give them a chance and subjected also these materials to paleointensity determinations, specially to the Nealtican ceramic sherds since these are unique samples.

Seven, six and six specimens from the site PO-3 (Nealtican), site PO-4 (Xalitzintla) and site PO-5 (Buenavista) lava flows, respectively, were treated with the TC protocol. In the case of the PDCs, nine specimens coming from two different scoria clasts (site PO-1) and twelve specimens coming from three different scoria clasts (PO-2) were analyzed using the same protocol. Data were analyzed with the ThellierTool4.0 software (Leonhardt et al. 2004).

All analyzed specimens from the site PO-3 lava flow yielded reliable results, with associated mean fraction (*f*), gap (*g*) and quality (*q*) parameters of 0.71, 0.84 and 16.0, respectively. Mean raw PI for this lava flow is 60.3 ± 2.6 μT ($n = 7$), while the cooling rate-corrected mean value is 57.4 ± 3.8 μT ($n = 7$). Results for the site PO-3 lava flow are listed in Table 2, together with their corresponding quality parameters, while a representative Arai plot is shown in Fig. 16a.

No positive results from the site PO-4 and site PO-5 specimens could be obtained. In the case of the site PO-5 lava flow, unsuccessful results could be attributed to (1), strong secondary components of some specimens likely caused by lightning strikes. This fact is evidenced at the NRM versus *k* plot (Fig. 6), where specimens from the Buenavista lava plot between the constant lines $Q = 10$ and $Q = 100$. (2) Points at the Arai plot define a typical concave-up behavior, characteristic of multidomain remanence carriers, and (3) the significant contribution to the magnetization carried likely by Ti maghemite, which transforms to Ti magnetite upon heating up to 600 °C. In the case of the site PO-4 lava flow, Arai plots are characterized by a relatively fast NRM lost without corresponding TRM acquisition for the six specimens that failed to produce a PI estimate.

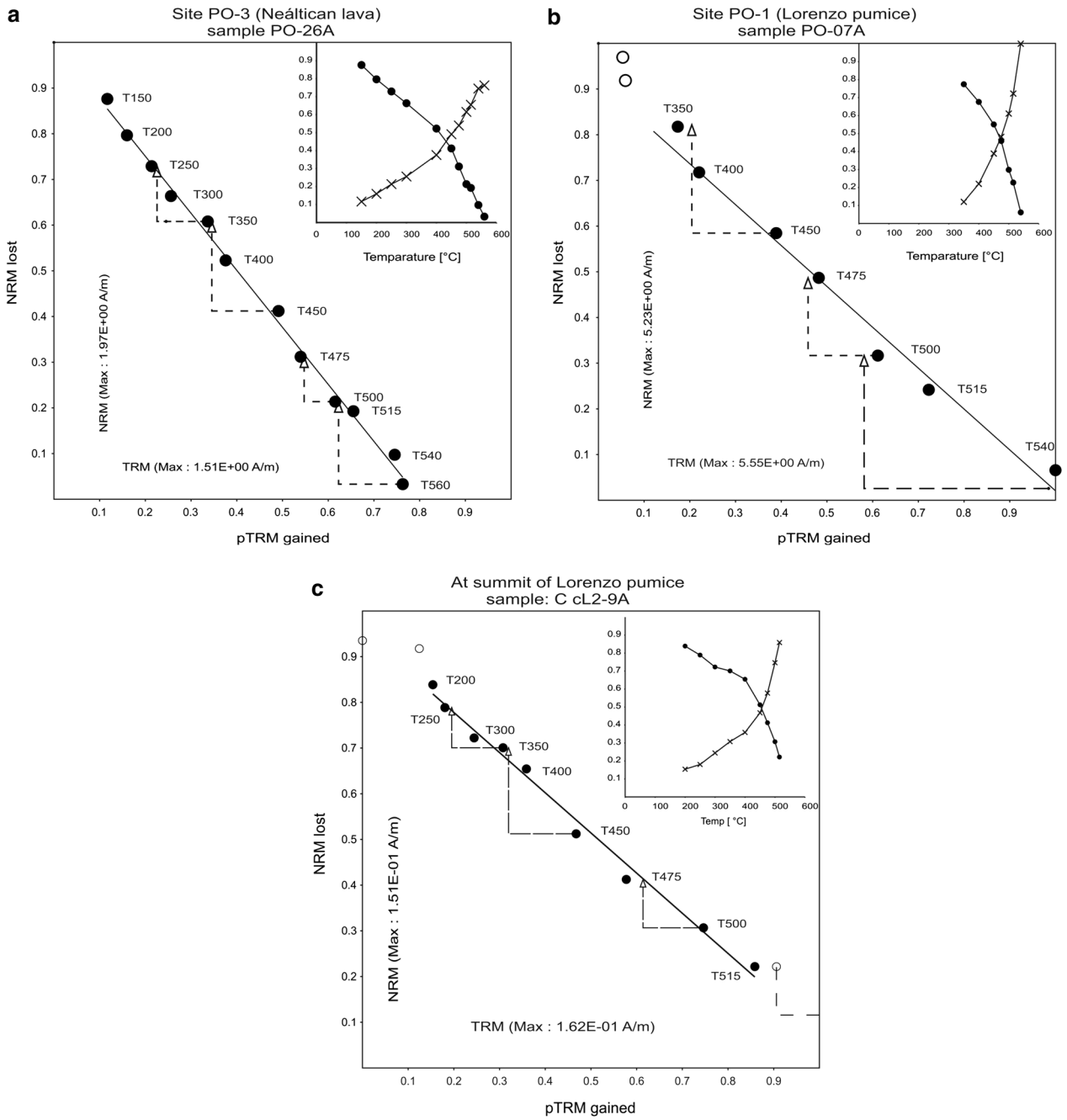

Fig. 16 **a**–**c** Representative Thellier–Coe NRM lost versus pTRM gained (Arai) plots for the different studied flows. Neáltica lava (**a**), Lorenzo Pumice flow (**b**) and summit of Lorenzo Pumice (**c**). Filled circles correspond to data points obtained at each double heating step used for the best fit regression line. Open circles correspond to data points not considered for the best fit calculation. Inset shows the NRM lost (pTRM gain) versus temperature at each step. Triangles represent the pTRM checks

For the *Lorenzo Pumice* (site PO-1), 9 specimens produced reliable results. However, 3 specimens yielded a high PI value of 69.2 ± 4.2 μT, while the other 6 specimens a lower PI value of 43.8 ± 2.8 μT. A representative Arai plot is shown in Fig. 16b. For the *Pink Pumice* (site PO-2), nine out of 12 specimens produced reliable results. In this case, PI values of 54.9 ± 3.4 μT ($N=5$), 45.4 ± 2.8 μT ($N=3$) and 62.9 ± 3.5 μT ($N=2$) were obtained for the three different sampled clasts. Results for the sites PO-1 and PO-2 are listed in Table 3.

Table 3 Thellier–Coe paleointensity results for sites PO-1 and PO-2 (pyroclastic density currents)

Specimen	ΔT (°C)	N	β	f	g	q	δ(CK)	δ(TR)	MAD_{anc}	Class	H_{raw} (μT)	$\pm\sigma H$ (μT)	f	H_{crc} (μT)
Site PO-1														
Clast 1														
1B	250–560	9	0.05	0.52	0.60	7.7	1.4	5.9	1.5	C	65.41	2.68	1.00	65.18
2B	250–560	9	0.07	0.42	0.68	4.1	4.4	2.9	1.2	B	69.93	4.83	1.02	66.59
3A	400–560	6	0.04	0.29	0.54	4.0	4.7	5.7	1.4	C	73.74	2.91	1.00	73.37
									Mean =		69.7			69.2
									1σ =		4.2			4.2
Clast 2														
4A	250–560	9	0.01	0.50	0.59	3.0	3.2	4.4	1.1	B	44.29	1.39	1.00	44.29
4B	250–560	9	0.04	0.57	0.55	7.7	3.6	4.8	0.9	A	41.23	1.86	1.00	41.23
5A	250–560	9	0.05	0.69	0.44	5.9	2.6	5.3	1.1	B	44.32	1.67	1.08	41.01
6A	300–560	8	0.03	0.87	0.77	19.0	0.4	8.6	1.1	C	42.15	2.19	1.02	41.50
8A	250–560	9	0.03	0.88	0.82	26.8	9.0	6.8	1.7	C	42.42	1.30	1.00	42.51
9A	250–560	9	0.05	0.91	0.81	15.4	1.6	9.7	0.9	C	45.17	2.40	1.00	45.17
									Mean =		44.5			43.8
									1σ =		3.7			2.8
Site PO-2														
Clast 1														
10A	*200–540*	*8*	*0.06*	*0.72*	*0.77*	*9.1*	*18.0*	*5.5*	*1.3*	*C*	*57.7*	*3.84*	*1.00*	*57.7*
11A	150–515	7	0.12	0.36	0.66	1.9	0.5	2.8	1.2	*B*	57.6	7.1	1.01	57.0
12A	200–515	9	0.05	0.37	0.67	4.6	7.6	2.8	1.0	*B*	58.7	3.14	1.04	56.4
13A	200–515	8	0.10	0.38	0.65	2.5	4.2	4.5	0.9	*B*	59.2	5.93	1.05	56.4
14A	150–515	8	0.12	0.32	0.64	1.8	3.7	6.5	0.7	*B*	50.1	5.91	1.01	49.8
									Mean =		56.4			54.9
									1σ =		4.1			3.4
Clast 2														
15A	200–515	9	0.07	0.35	0.78	3.9	6.3	1.5	1.8	B	48.05	3.33	1.04	46.2
16B	300–560	9	0.09	0.35	0.79	3.0	42.9	3.6	1.5	C	50.00	4.67	1.05	47.6
17A	250–560	7	0.08	0.31	0.85	3.1	62.0	4.4	1.1	C	42.74	3.59	1.01	42.3
18A	N/R	–	–	–	–	–	–	–	–		–	–		–
									Mean =		46.9			45.4
									1σ =		3.8			2.8
Clast 3														
19B	350–540	7	0.07	0.37	0.82	4.0	9.4	5.7	4.1	B	68.68	4.28	1.05	65.4
20A	200–540	9	0.05	0.49	0.87	8.3	7.6	4.9	2.1	B	64.10	1.46	1.06	60.5
20B	N/R	–	–	–	–	–					–	–	–	–
									Mean =		66.4			62.9
									1σ =		3.2			3.5

Data in italics not used for PI calculations

ΔT temperature interval used for the intensity determination, N number of heating steps used for the intensity determination, $\beta = \sigma m/m$, f fraction of extrapolated NRM used for intensity determination, g gap factor, q quality factor as defined by Coe et al. (1978), δ(CK), δ(TR), MAD_{anc} and class as defined by Leonhardt et al. (2004), H_{raw} raw archeointensity value, σH standard deviation of H, f cooling rate correction factor, H_{crc} cooling rate-corrected archeointensity

Only three out of the eight analyzed ceramics fragments—four unearthed from the *Lorenzo Pumice* (labeled dL) and four at its summit (labeled cL)—yielded reliable PI results. As in the case of samples from the lava flow site PO-3, symmetrical NRM lost and pTRM gained plots were obtained during the TC paleointensity experiments. Mean quality parameters of $f=0.61$, $g=0.82$ and $q=13.1$, and an associated anisotropy-corrected mean PI $=39.1\pm1.5$ μT ($N=6$) were obtained for the fragment cL2 at the summit. For the ceramic fragment dL2, mean quality parameters of $f=0.47$, $g=0.80$ and $q=8.1$, and an associated anisotropy-corrected mean PI $=30.7\pm2.5$ μT ($N=5$) were obtained,

Table 4 Thellier–Coe paleointensity results for ceramic fragments

Spec	ΔT (°C)	N	β	f	g	q	δ(CK)	δ(TR)	MAD_{anc}	Class	H_{raw} (μT)	$\pm\sigma H$ (μT)	f_{ani}	H_{ani}
cL2–7	150–515	10	0.06	0.59	0.86	8.4	15.6	1.1	0.8	C	47.1	2.87	0.865304	40.8
cL2–8	250–515	8	0.03	0.55	0.84	14.6	15.3	0.8	1.3	C	43.7	1.47	0.894808	39.1
cL2–9	250–515	8	0.04	0.61	0.84	11.7	7.8	1.3	1.2	B	43.4	1.67	0.875342	38.0
cL2–10	150–515	10	0.05	0.73	0.86	12.8	6.9	2.8	1.7	B	43.5	2.06	0.866909	37.7
cL2–11	350–515	6	0.05	0.58	0.78	8.9	2.0	6.0	1.9	A	47.7	2.30	0.861864	41.1
cL2–12	350–515	6	0.02	0.60	0.77	22.0	5.2	5.1	2.3	B	39.8	0.81	0.954895	38.0
									Mean =		44.2			39.1
									1σ =		2.9			1.5
dL2–30	350–540	7	0.11	0.51	0.82	3.9	6.4	1.7	7.8	B	31.8	3.5	0.953086	30.3
dL2–31	350–515	6	0.06	0.43	0.78	5.2	2.2	7.5	4.9	B	38.9	2.5	0.976721	38.0
dL2–32	N/R	0	–	–	–	–	–	–	–		–	–	0.975110	31.8
dL2–33	350–515	6	0.04	0.47	0.77	9.0	3.7	6.8	3.5	B	32.4	1.3	0.981138	28.0
dL2–34	350–540	7	0.10	0.53	0.80	4.3	7.2	16.0	5.8	C	32.6	3.2	0.859148	30.6
dL2–35	350–475	4	0.06	0.30	0.66	3.4	3.9	4.6	3.4	C	34.2	2.0	0.896152	
									Mean =		34.0			31.7
									1σ =		2.9			3.7
dL3–36	300–515	7	0.04	0.27	0.76	4.9	2.7	2.2	1.6	C	54.6	2.2	0.932281	50.9
dL3–38	300–515	7	0.10	0.27	0.70	1.9	2.3	0.3	1.6	C	50.1	5.1	0.906250	45.4
dL3–39	N/R	–	–	–	–	–	–	–	–	C	–	–	0.964768	54.9
dL3–40	N/R	–	–	–	–	–	–	–	–		–	–		
dL3–41	300–475	5	0.08	0.21	0.72	1.9	2.8	2.0	1.9		56.9	4.5		
									Mean =		53.9			50.4
									1σ =		3.4			4.8

Spec: cL2: summit of Lorenzo pumice; dL2 and dL3: below Lorenzo pumice

ΔT temperature interval used for the intensity determination, N number of heating steps used for the intensity determination, $\beta = \sigma m/m$, f fraction of extrapolated NRM used for intensity determination, g gap factor, q quality factor as defined by Coe et al. (1978), δ(CK), δ(TR), MAD_{anc} and class as defined by Leonhardt et al. (2004), H_{raw} raw archeointensity value, σH standard deviation of H_{raw}, f_{ani} anisotropy correction factor, H_{ani} anisotropy-corrected archeointensity

while for the ceramic fragment dL3 corresponding mean quality parameters of $f=0.36$, $g=0.83$ and $q=7.1$, and an associated anisotropy-corrected mean PI $=40.1\pm1.3$ μT ($N=2$) were obtained. PI results for the ceramic fragments are listed in Table 4, together with their corresponding quality parameters, and a representative Arai plot is shown in Fig. 16c. For the other five ceramics fragments erratic behavior of the NRM was evidenced after each zero-field step during the TC experiments. PI estimates were abnormally low or high. Results of magnetic susceptibility measurements of lava specimens after each double heating-step during the Thellier-Coe PI experiments are shown in Additional file 1. Those corresponding to ceramic shards are shown in Additional file 2.

Paleomagnetic dating

The most probable date for the cooling of the analyzed lava flows (paleomagnetic dating) was determined by assessment of the corresponding probability density function (PDF) obtained by the of use the Matlab tool *archaeo_dating*, developed by Pavón Carrasco et al. (2011), along with the global model SHA.DIF.14 k (Pavón Carrasco et al. 2014) calculated for the geographical position of the sites. This model is the latest developed using all the available paleomagnetic data for their corresponding time intervals and applying the classical modeling approach, i.e., the spherical harmonic analysis in space and the penalized cubic B-splines in time. Full-vector paleomagnetic dating of site PO-3 yields the single time interval of AD 1038–AD 1139 as the most probable age for the lava's cooling moment (Fig. 17). Paleointensity dating of pottery shard cL2 (Fig. 18) yields a time interval of AD 584–AD 823, locating it in time at the Epiclassic period.

Discussion

Rock-magnetism and paleomagnetism

Volcanic rocks are recognized as good geomagnetic field recorders (e.g., Morales et al. 2010 and references therein), and although at field work the lava flows sampled looked fresh and without evidence of alteration, only one out of the three lava flows sampled yielded reliable results, both in direction and in intensity. This successful flow (site PO-3) locates at an altitude of ~2300 m a.s.l.,

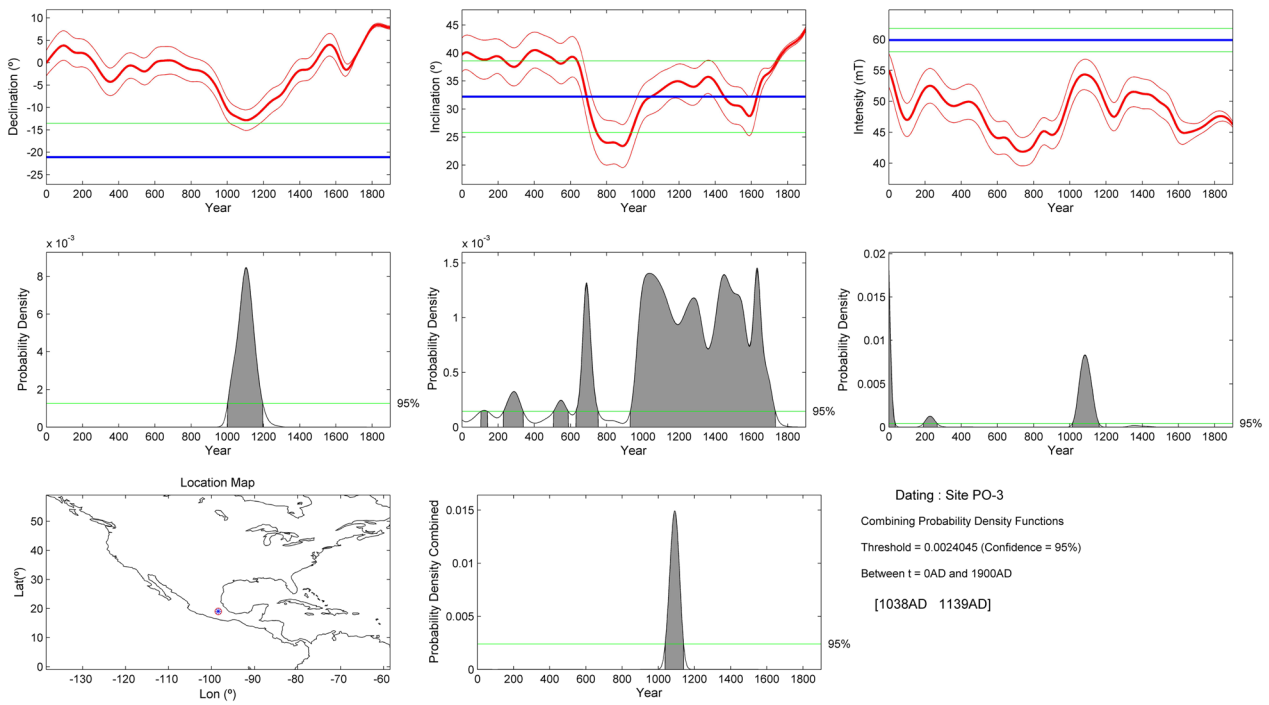

Fig. 17 Full-vector paleomagnetic dating of the Nealtican (1 k) lava flow. Upper panels: red thick curves show the variation in time of the directional (declination and inclination) and magnitude (intensity) components of the paleomagnetic field as determined from the SHA.DIF.14 k model, while blue thick horizontal lines represent the mean declination, inclination and intensity of the ancient field determined in laboratory. All curves/lines are shown with their corresponding 95% confidence intervals (thin curves/lines above and below the corresponding thick curves/line). Central panels: The corresponding probability density functions are shown as shaded peaks, together with the 95% confidence level highlighted by horizontal green lines. The combined (Dec, Inc and intensity) probability density is shown at the lower most right panel

while the other two (unsuitable) lava flows at ~2700 (site PO-4) and above 3400 m a.s.l. (site PO-5), respectively.

The several strong secondary components shown by samples coming from site PO-5 (Fig. 13e), explained as of isothermal origin (IRMs), could be well explained in terms of lightings—very common at high altitudes—also evidenced by the high values at the Königsberger plot (Fig. 6). Moreover, the rather irreversible M–T plot of the Buenavista lava and the multiple minerals phases with T_c of ~160, 270, 360 and 560 °C could account for the unsuccessful results obtained for this lava flow.

On the other hand, the relatively fast NRM lost without corresponding TRM acquisition for the six specimens that failed to produce a PI estimate for site PO-4 could be explained by irreversible motion of domain walls during successive heating and cooling experiments (Levi 1977). Alternatively, this behavior may result from irreversible variations of coercive force (Kosterov and Prévot 1998) at low temperatures, and can be interpreted as transformation from a single-domain "metastable" state to a multidomain state, which results in large NRM lost without any correlated pTRM acquisition.

In a previous study, Conte et al. (2004) reported the paleodirectional and paleointensity study of 16 Popocatepetl lava flows, for which a mean paleodirection with $D=345.7°$, $I=35.4°$, $k=21$, $\alpha_{95}=8.5°$, $N=15$ was obtained. However, most of these lavas were sampled at the northern sector of the edifice, while ours at the northeastern flank. Mean paleodirection obtained for site PO-3 agrees with that reported by Conte et al. (2004). In regard to the unexpected high inclination value (49.2°) obtained for site PO-1, we note that five out of the 16 lava flows studied by Conte et al. (2004) present even higher inclination values (48.9°–69.5°). On the other hand, only four individual lava flows (fourteen samples) yielded acceptable paleointensity estimates which yielded mean-flow paleointensity values in the range from 30.2 ± 7.3 to 46.9 ± 5.6 μT.

Estimation of emplacement temperatures of PDCs

In a paleomagnetic and rock-magnetic investigation carried out on scoria clasts sampled from three historically active volcanoes—Láscar in the Chilean Andes, Mt. St. Helens, USA and Vesuvius, Italy—Paterson et al. (2010)

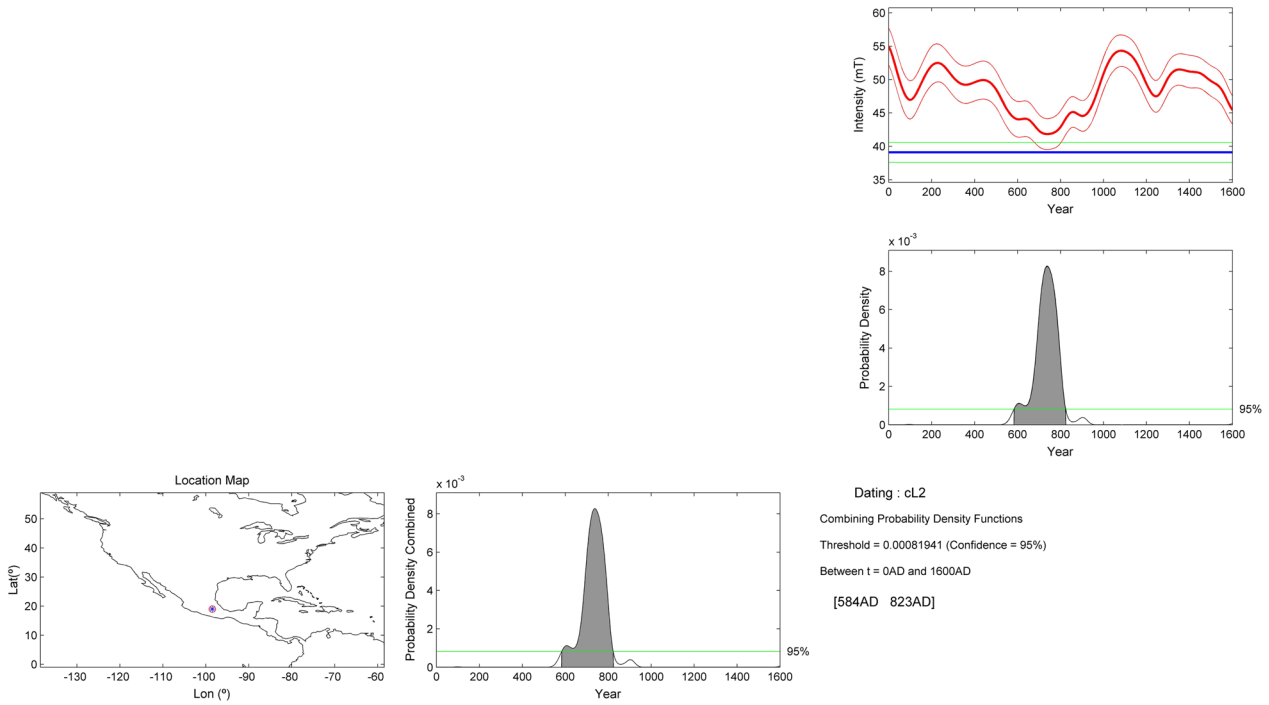

Fig. 18 Paleointensity dating for the pottery shard cL2 based on a mean PI = 38.9 ± 2.6 μT obtained from five specimens. Description of the different panels as in Fig. 17

highlighted the usefulness of lithic clasts from pyroclastic deposits for paleointensity determination.

In this investigation, seven out of nine specimens coming from two different scoria clasts of PDC PO-1 yielded a well-constrained direction (Dec = 337.3°, Inc = 49.2°, $\alpha_{95} = 4.5°$), although with a high inclination. Three specimens yielded a high PI value of 69.2 ± 4.2 μT, while the other 6 specimens yielded a lower PI value of 43.8 ± 2.8 μT. Single-magnetization Zijderveld plots and well-grouped paleomagnetic direction of the seven specimens from the two different scoria clasts of PDC PO-1 (*Lorenzo Pumice*, Fig. 15a) suggest that clasts were emplaced hot, at a temperature that seems to have completely reset the original magnetization of the clasts, and then cooled in situ after deposition. Nonetheless, one or both lithologies seem to have experienced alteration due to reheating, anisotropy of remanence effects affected different to both clasts, or a combination of both cases resulted in different intensities records of the Earth's magnetic field present during emplacement.

In case of site PO-2 (Pink Pumice), the three clusters roughly concentrated around the present geomagnetic field (Fig. 15b). This could suggest that the PDC was emplaced also at high temperature—as high as that estimated for site PO-1—and that movement during or after the emplacement resulted in a slightly scattered mean direction.

Pottery shard cL2 seems to have not experienced a post-deposition heating, as evidenced by the single-magnetization vectorial plot (Fig. 15a) (see also Additional file 3: *THD cL Ceramics*). Nonetheless, it should be considered that despite the high temperature of the PDC the pottery fragments were not re-heated because they were covered (protected) by the soil.

Pottery shards dL2 and dL3, unearthed below the—hot-emplaced—*Lorenzo Pumice* deposit, show results of the reheating as a clear secondary low-temperature range (room temperature to ~300–350 °C) component at the orthogonal plot (Fig. 15b) (see also Additional file 4: *THD dL Ceramics*). Likely, this reheating could be acquired during its continues usage as an utilitarian piece. However, as above mentioned, some of the shards likely come from an ornamental tripod vase. Moreover, differences in the color of the fragments can be observed; thus, they probably correspond to different ceramic artifacts. Therefore, most ceramics shards must come from an ornamental (heated just once during its elaboration) rather than from a utilitarian artifact.

Conclusions

New paleomagnetic results from Popocatepetl volcano are reported. Full-vector (direction and intensity) paleomagnetic dating of the Nealtican lava obtained (for the first time) confirms the ^{14}C date for this fissural lava flow. Reliable new paleointensity results on scoria clasts from PDCs were obtained (also for the first time) for Popocatepetl volcano. Estimated emplacement temperatures for the PDCs of the Lorenzo and Pink Pumice indicate that clasts were emplaced hot, above the T_c of magnetite (580 °C).

Additionally, first archeointensity dating of pottery shards within pyroclastic density currents of Popocatepetl volcano is reported.

As claimed in most paleointensity investigations, alteration both in nature or during laboratory heating and the influence of MD grains were the main factors of failure to experimentally determine the paleointensity in the other two lava flows.

Finally, results of the rock-magnetic and paleomagnetic dating of the last Plinian eruptions from Popocatepetl volcano, applied to different volcanic materials—lava and pyroclastic density currents—show the usefulness of these nonconventional and alternative techniques in the study of the eruptive activity of volcanoes. Both scoria clast and pottery shard within PDCs provide useful information about the ancient geomagnetic field, as well as emplacement temperatures of pyroclastic density currents.

Additional files

Additional file 1. Susceptibility vs Temperature of ceramic shards. Excel file with the results of magnetic susceptibility measurements of the lava specimens after each double heating-step during the Thellier-Coe paleointensity experiments. At the top of the first sheet are shown the raw data, while at the bottom part the normalized susceptibility values. In the second sheet the normalized Susceptibility vs Temperature plots for each ceramic shard analyzed are shown.

Additional file 2. Susceptibility vs Temperature of ceramic shards. Excel file with the results of magnetic susceptibility measurements of the ceramic shards after each double heating-step during the Thellier-Coe paleointensity experiments. At the top of the first sheet are shown the raw data, while at the bottom part the normalized susceptibility values. In the second sheet the normalized Susceptibility vs Temperature plots for each ceramic shard analyzed are shown.

Additional file 3. THD cL2 Ceramics: Thermal demagnetization results for representative shards buried by the UCPE pyroclastic density current. Figure includes normalized intensity decay curves (left), Zijderveld diagrams (middle) and corresponding equal-area projections (right). Most specimens displayed mainly a single paleomagnetic component directed through the origin, accompanied by an initial weak overprint of possibly viscous origin which could be removed at fields/temperatures below 10 mT/150 °C. Symbols: Zijderveld diagram: full/open dot, declination/apparent inclination; equal-area projection: full/open dot, positive/negative inclination.

Additional file 4. THD dL2 Ceramics: Thermal demagnetization results for representative shards buried by the LCPE pyroclastic density current. Figure includes normalized intensity decay curves (left), Zijderveld diagrams (middle) and corresponding equal-area projections (right). Arrows indicate the temperature step corresponding to the reheating of the ceramic shards. Symbols: Zijderveld diagram: full/open dot, declination/apparent inclination; equal-area projection: full/open dot, positive/negative inclination.

Abbreviations

TMVB: trans-Mexican volcanic belt; UPCPE: Upper Pre-ceramic Plinian eruption; LCPE: Lower Ceramic Plinian eruption; UCPE: Upper Ceramic Plinian eruption; AI: archeointensity; PI: paleointensity; AVFTB: advance variable field translation balance; AF: alternating field; ARM: anhysteretic remanent magnetization; ChRM: characteristic remanent magnetization; IRM: isothermal remanent magnetization; NRM: natural remanent magnetization; TRM: thermoremanent magnetization; pTRM: partial thermoremanent magnetization; TC: Thellier–Coe; T_c: Curie temperature; CR: cooling rate; SD: single domain; PSD: pseudo-single domain; MD: multidomain; Dec: declination; Inc: inclination; PDF: probability density function.

Acknowledgements

The exhaustive and constructive revisions of two anonymous reviewers are greatly acknowledged.

Authors' contributions

NP-R participated in the field work, sample preparation and measurement of samples. JM participated in the field work, supervised the experimental procedures and participated in the analysis and interpretation of results and the writing of the manuscript. AG participated and supported the field work via his project. FG-T participated in the field work. All authors read and approved the final manuscript.

Funding

AG is grateful for financial support of UNAM-PAPIIT Project 101717.

Availability of data and materials

The datasets used and/or analyzed during the current study are available from the corresponding author on reasonable request.

Ethics approval and consent to participate

Not applicable.

Consent for publication

Not applicable.

Competing interests

The authors declare that they have no competing interests.

Author details

[1] Posgrado en Ciencias de la Tierra, UNAM, Unidad Michoacán, Campus Morelia, Antigua Carretera a Pátzcuaro No. 8701 Col. Ex-Hacienda de San José de la Huerta, 58190 Morelia, Michoacán, Mexico. [2] Laboratorio Interinstitucional de Magnetismo Natural (LIMNA) y Servicio Arqueomagnético Nacional (SAN), Instituto de Geofísica, UNAM, Unidad Michoacán, Campus Morelia, Antigua Carretera a Pátzcuaro No. 8701 Col. Ex-Hacienda de San José de la Huerta, 58190 Morelia, Michoacán, Mexico. [3] Instituto de Geofísica, UNAM, Unidad Michoacán, Campus Morelia, Antigua Carretera a Pátzcuaro No. 8701 Col. Ex-Hacienda de San José de la Huerta, 58190 Morelia, Michoacán, Mexico.

Received: 25 February 2019 Accepted: 11 July 2019
Published online: 29 July 2019

References

AGICO Prints (2018) Anisotropy of magnetic remanence a brief practical guide application note. https://www.agico.com/. Accessed 6 Sep 2018

Anisoft5 (2018) Anisotropy data browser. Version 5.1.01. https://www.agico.com/text/software/anisoft/anisoft.php. Accessed 6 Apr 2018
Arana-Salinas L, Siebe C, Macías JL (2010) Dynamics of the ca. 4965 ^{14}C BP "Ochre Pumice" Plinian eruption of Popocatépetl volcano, México. J Volcanol Geoth Res 192:212–231
Bardot L (2000) Emplacement temperature determinations of proximal pyroclastic deposits on Santorini Greece, and their implications. Bull Volcanol 61:450–467
Carrasco-Nuñez G, Silva L, Delgado-Granados H, Urrutia-Fucugauchi J (1986) Geologia y paleomagnetismo del Popocatepetl: Mexico, DF. UNAM Publ Ser Inv Inst Geofis, No 33
Chadima M, Hrouda F (2006) Remasoft 3.0—a user-friendly paleomagnetic data browser and analyzer. Travaux Géophysiques XXVII:20–21
Chauvin A, Garcia Y, Lanos P, Laubenheimer F (2000) Paleointensity of the geomagnetic field recovered on archaeomagnetic sites from France. Phys Earth Planet Inter 120:111–136
Coe RS (1967) Paleo-intensities of the Earth's magnetic field determined from tertiary and quaternary rocks. J Geophys Res 72(12):3247–3262
Coe RS, Grommé S, Mankinen EA (1978) Geomagnetic paleointensities from radiocarbon dated lava flows on Hawaii and the question of the Pacific nondipole low. J Geophys Res 83:1740–1756
Conte G, Urrutia-Fucugauchi J, Goguitchaichvili A, Soler-Arechalde AM, Morton-Bermea O (2004) Paleomagnetic Study of Lavas from the Popocatepetl Volcanic Region, Central Mexico. Int Geol Rev 46(2004):210–225
Day R, Fuller M, Schmidt V (1977) Hysteresis properties of titanomagnetites: grain-size and compositional dependence. Phys Earth Planet Inter 13:260–266
Di Vito MA, Zanella E, Gurioli L, Lanza R, Sulpizio R, Bishop J, Evdokia T, Boenzi G, Laforgia E (2009) The Afragola settlement near Vesuvius, Italy: the destruction and abandonment of a Bronze Age village revealed by archaeology, volcanology and rock-magnetism. Earth Planet Sci Lett 277:408–421
Dunlop DJ (2011) Physical basis of the Thellier-Thellier and related paleointensity methods. Phys Earth Planet Inter 187(3–4):118–138. https://doi.org/10.1016/j.pepi.2011.03.006
Ferrari L (2000) Avances en el conocimiento de la Faja Volcánica Transmexicana durante la última década. Boletín de la Sociedad Geológica Mexicana LIII:84–92
Gómez-Tuena A, Orozco-Esquivel MT, Ferrari L (2005) Petrogénesis Ígnea de la Faja Volcánica Transmexicana. Boletín de la Sociedad Geológica Mexicana LVII(3):227–233
Hagstrum JT, Champion DE (2002) A Holocene paleosecular variation record from 14C dated volcanic rocks in western North America. J Geophys Res 107:2025. https://doi.org/10.1029/2001JB000524(B1)
Kosterov A, Prévot M (1998) Possible mechanisms causing failure of Thellier palaeointensity experiments in some basalts. Geophys J Int 134:554–572
Kosterov A, Conte G, Goguitchaichvili A, Urrutia-Fucugauchi J (2009) Low-temperature magnetic properties of andesitic rocks from Popocatepetl stratovolcano, Mexico. Earth Planets Space 61:133–142. https://doi.org/10.1186/BF03352893
Leonhardt R (2006) Analyzing rock magnetic measurements: the Rock-MagAnalyzer 1.0 software. Comput Geosci 32:1420–1431
Leonhardt R, Heunemann C, Krása D (2004) Analyzing absolute paleointensity determinations: acceptance criteria and the software ThellierTool4.0. Geochem Geophys Geosyst 5(12):Q12016. https://doi.org/10.1029/2004GC000807
Levi S (1977) The effect of magnetite particle size on paleointensity determination of the geomagnetic field. Phys Earth Planet Inter 13:245–259
Macías JL (2005) Geología e historia eruptiva de algunos de los grandes volcanes activos de México. Boletín de la Sociedad Geológica Mexicana, Volumen Conmemorativo del Centenario LVII(3):395–399
McClelland E, Druitt TH (1989) Palaeomagnetic estimates of emplacement temperatures of pyroclastic deposits on Santorini Greece. Bull Volcanol 51:16–27
Morales J, Goguitchaichvili A, Acosta G, González-Morán T, Alva-Valdivia L, Robles-Camacho J, Hernández-Bernal MS (2009) Magnetic properties and archeointensity determination on Pre-Columbian pottery from Chiapas, Mesoamerica. Earth Planets Space. https://doi.org/10.1186/BF03352887
Morales J, Zhao X, Gogichaishvili A (2010) Geomagnetic field intensity from Kilauea 1955 and 1960 lava flows: toward a better understanding of paleointensity. Stud Geophys Geod 54:561–574
Panfil M, Gardner T, Hirth K (1999) Late Holocene stratigraphy of the Tetimpa archaeological sites, northeast flank of Popocatépetl volcano, central Mexico. GSA Bull 111(2):204–218
Paterson GA, Muxworthy AR, Roberts AP, Mac Niocaill C (2010) Assessment of the usefulness of scoria clasts from pyroclastic deposits for paleointensity determination. J Geophys Res 115:B03104. https://doi.org/10.1029/2009JB006475
Pavón Carrasco FJ, Rodríguez-González J, Osete ML, Torta JM (2011) A Matlab tool for archeomagnetic dating. J Archaeol Sci 38:408–419
Pavón Carrasco FJ, Osete ML, Torta JM, De Santis A (2014) A geomagnetic field model for the holocene based on archeomagnetic and lava flow data. Earth Planet Sci Lett 388:98–109
Plunket P, Uruñuela G (1998) Preclassic household patterns preserved under Volcanic Ash at Tetimpa, Puebla, Mexico. Latin Am Antiq 9(4):287–309
Riisager P, Riisager J (2001) Detecting multidomain magnetic grains in Thellier palaeointensity experiments. Phys Earth Planet Inter 125:111–117
Robin C (1984) Le Volcan Popocatépetl (Mexique): strecture, evolution pétrologique et risques. Bull Volcanol 47:1
Schaaf P, Stimac J, Siebe C, Macías JL (2005) Geochemical evidence for mantle origin and crustal processes from products of Popocatépetl and surrounding monogenetic volcanoes. J Petrol 46:1243–1282
Selkin PA, Gee JS, Tauxe L, Meurer WP, Newell AJ (2000) The effect of remanence anisotropy on paleointensity estimates: a case study from the Archean Stilleater Complex. Earth Planet Sci Lett 183:403–416
Siebe C, Macías JL (2006) Volcanic hazards in the Mexico City metropolitan area from eruptions at Popocatépetl, Nevado de Toluca, and Jocotitlán stratovolcanoes and monogenetic scoria cones in The Sierra Chichinautzin Volcanic Field. The Geological Society of America, Boulder, pp 1–33
Siebe C, Macías JL, Abrams M, Rodríguez S, Castro R, Delgado H (1995) Quaternary explosive volcanism and pyroclastic deposits in east central Mexico: implications for future hazards. In: Chacko J (ed) Guidebook for the 1995 annual meeting of the Geological Society of America. Geological Society of America, New Orleans, Louisiana, pp 1–47
Siebe C, Macías JL, Abrams M, Obenholzner J (1996a) La destrucción de Cacaxtla y Cholula: un suceso en la historia eruptiva del Popocatépetl. Ciencias 41:36–45
Siebe C, Macías JL, Abrams M, Obenholzner J (1996b) Repeated volcanic disaster in Prehispanic time at Popocatépetl, central México: past key to the future? Geology 24(5):399–402
Sosa-Ceballos G, Macías JL, García-Tenorio F, Layer P, Schaaf P, Solís-Pichardo G, Arce JL (2015) El Ventorrillo, a paleostructure of Popocatépetl volcano: insights from geochronology and geochemistry. Bull Volc 77:2–20
Tema E (2009) Estimate of the magnetic anisotropy effect on the archaeomagnetic inclination of ancient bricks. Phys Earth Planet Inter 176:213–223
Tema E, Zanella E, Pavón-Carrasco FJ, Kondopoulou D, Pavlides S (2015) Palaeomagnetic analysis on pottery as indicator of the pyroclastic flow deposits temperature: new data and statistical interpretation from the Minoan eruption of Santorini, Greece. Geophys J Int 203:33–47
Thellier E, Thellier O (1959) Sur l'intensité du champ magnétique terrestre dans le passé historique et géologique. Ann Géophys 15:285–376
Zanella E, Gurioli L, Lanza R, Sulpizio R, Bontempi M (2008) Deposition temperature of the AD 472 Pollena pyroclastic density current deposits, Somma-Vesuvius, Italy. Bull Volcanol 70:1237–1248

Publisher's Note